Subsidence pattern in the central Adriatic and its influence on sediment architecture during the last 400 kyr

V. Maselli,[1,2] F. Trincardi,[2] A. Cattaneo,[3] D. Ridente,[4] and A. Asioli[5]

Received 6 May 2010; revised 10 August 2010; accepted 25 August 2010; published 28 December 2010.

[1] The western Adriatic margin (eastern Mediterranean), part of the Apennine foreland, is characterized by a differentiated tectonic setting, showing high subsidence rates (up to 1 mm/yr) in the northern area and tectonic uplift (on the order of 0.3–0.5 mm/yr) in the southern part corresponding with the so-called Apulia swell. The central Adriatic marks the transition between these two areas. To calculate subsidence values, the stratigraphy of the central Adriatic has been investigated through the borehole PRAD1.2 (European project Profiles across Mediterranean Sedimentary Systems), the first continuous Quaternary marine record in the Adriatic basin (71.2 m long) reaching the top of Marine Isotope Stage 11 (MIS 11). Subsidence calculations were performed first by applying the backstripping procedure to PRAD1.2, in order to investigate the contribution of sediment load and tectonic driving forces to subsidence. Despite the large error bars, mostly caused by the uncertainties in paleowater depth reconstructions, the values obtained demonstrate that tectonics is the main driver for subsidence in this area. In order to better estimate the subsidence rates, an independent approach is introduced, based on the correlation of the present-day burial depth of past shorelines deposited during the main glacial lowstands, from MIS 2 to MIS 10. The average subsidence rate of about 0.3 mm/yr appears greater than the average sediment supply rate (0.15 mm/yr), and this fact explains the overall backstepping of the 100 kyr regressive depositional sequences on the margin. The results obtained help to improve the understanding of the regional tectonics and can be used for quantitative reconstruction of Quaternary sea level changes in the Adriatic region. In general, the paper shows that even a short (71 m) borehole across a relatively short time span (340 kyr) can be useful for subsidence calculations, provided that a high-resolution definition of its stratigraphy is available and a correlation can be drawn with the geomorphologic proxies such as paleoshoreline deposits.

Citation: Maselli, V., F. Trincardi, A. Cattaneo, D. Ridente, and A. Asioli (2010), Subsidence pattern in the central Adriatic and its influence on sediment architecture during the last 400 kyr, *J. Geophys. Res.*, *115*, B12106, doi:10.1029/2010JB007687.

1. Introduction

[2] Subsidence is one of the key factors controlling the filling pattern of sedimentary basins and, ultimately, the geometry of sedimentary successions. In order to understand and reconstruct the burial history of a sedimentary succession, *Van Hinte* [1978] introduced the "geohistory analysis," a simple analytical method that allows quantification of the total subsidence of a basin, and calculation of the contributions of sediment and water loads and of tectonic driving forces. In the last few decades the geohistory analysis has been performed with good results in a variety of geodynamic settings, but always referring to deep boreholes (on the order of a few kilometers) or long sedimentary sections, encompassing several millions of years [*Steckler and Watts*, 1978; *Sclater and Christie*, 1980; *Carminati et al.*, 2007]. Here we apply the geohistory analysis to the borehole PRAD1.2, a 71.2 m long borehole drilled in the central Adriatic margin, encompassing the last 400 kyr. The interest in applying this method on shorter timescales is in considering key factors controlling the evolution of a continental margin such as eustatic and sediment supply fluctuations, taking advantage of a precise (millennial scale) stratigraphic resolution available.

[3] In the last decades an increasing number of sites was drilled on Quaternary continental margins through rapidly deposited successions, with accumulation rates on the order of 1 mm/yr or higher [*Sydow and Roberts*, 1994; *Rabineau et al.*, 2006]. The European project Profiles across Mediterranean Sedimentary Systems (PROMESS1) was designed to investigate the impact of Quaternary sea level changes on the deposition of continental shelf and slope sequences

[1]Dipartimento di Scienze della Terra e Geologico-Ambientali, Univerisità di Bologna, Bologna, Italy.
[2]ISMAR, Istituto di Scienze Marine (CNR), Bologna, Italy.
[3]GM-LES, Ifremer, Plouzané, France.
[4]IGAG, CNR, Rome, Italy.
[5]IGG, CNR, Padova, Italy.

0148-0227/10/2010JB007687

on two Mediterranean margins: the Adriatic and the Gulf of Lion. Continuous-recovery drilling at site of high sedimentation rates and absence of marked erosional surface are fundamental to achieve the most complete paleoenvironmental and paleoclimatic reconstructions. The aim of this paper is to test the possibility to quantify the subsidence rates in the central Adriatic Sea from a high-resolution borehole over a short geological time interval (~400 kyr). We perform this test on a section of the Adriatic margin where subsidence rates are debated [*Colantoni et al.*, 1989; *Doglioni et al.*, 1994; *Ridente and Trincardi*, 2002; *Lambeck et al.*, 2004; *Ferranti et al.*, 2006; *Antonioli et al.*, 2009], in order to better explain the geometric relationships of depositional sequences during the Quaternary and their relation with eustatic and sediment supply fluctuations. The subsidence rates are first obtained through the geohistory analysis and using the backstripping method; the results obtained are then compared with another independent approach based on the identification of paleoshorelines formed during the main eustatic lowstands [*Skene et al.*, 1998].

2. Geologic and Stratigraphic Framework

2.1. Geological Setting

[4] The Adriatic Sea is a semienclosed basin elongated in the NW–SE direction with a length of 800 km and a width of 200 km, showing a remarkable variability in shelf and slope morphology. The shelf break is about 300 km away from the Gulf of Venice, and the shelf presents a gentle dip of about 0.02° toward the SE. The Mid Adriatic Deep (MAD), south of the shelf break, represents a small remnant basin with a maximum depth of 260 m that has been progressively filled from the NW by the Po River delta deposits during each Quaternary phase of sea level fall and lowstand; the last progradational wedge originated during the Last Glacial Maximum [*Cattaneo and Trincardi*, 1999; *Asioli et al.*, 2001]. In the central Adriatic the continental shelf extends seaward about 50 km parallel to the front of the Apennine chain, with a seafloor dip of 0.3°–0.7°. The south Adriatic is a deeper basin showing a complex morphology and a maximum depth of about 1200 m (Figure 1). Overall, the Adriatic Sea is a mud-dominated system where the Po River is the most important source of sediment.

[5] During the last 25 Ma the westward subduction of the Adria plate led to the formation of the Apennine chain, while the Adriatic basin became a foreland domain. During the Pliocene and Pleistocene, the central Adriatic basin was characterized by a high subsidence rate because of the eastward rollback of the hinge of the Apennine subduction [*Royden et al.*, 1987]. The southern Adriatic basin was, instead, characterized by a different tectonic style, showing uplift since the middle Pleistocene [*Doglioni et al.*, 1994; *Scrocca*, 2006; *Ridente and Trincardi*, 2006]. This different tectonic behavior has been ascribed to differences in the thickness of the Adriatic lithosphere subducted toward the west [*Pieri and Groppi*, 1981; *Royden et al.*, 1987; *Doglioni et al.*, 1994].

[6] The modern foredeep basin in the central Adriatic is rimmed by two structures: the Gallignani-Pelagosa ridge (trending NW–SE), roughly parallel to the front of the Apennine chain, and the NE–SW Tremiti structural high, located north of the Gargano Promontory (Figure 1). The Tremiti lineament has been interpreted as the right-lateral transfer zone linking the pronounced eastward rollback of the central Adriatic slab and the buckled Apulian region [*Doglioni et al.*, 1994]. The stratigraphic and tectonic evolution of the central Adriatic since the Oligocene shows that the highest subsidence values are confined landward, toward the Apennine chain, as highlighted by the flexure of the Messinian datum corresponding to the evaporite unit and the related unconformity [e.g., *Scrocca*, 2006]. Since the middle Pleistocene, the units infilling the foredeep basin have changed from a dominant turbidite fill into a progradational margin wedge that records the Milankovich glacial-eustatic cyclicity [*Ridente et al.*, 2009].

2.2. PRAD1.2 Stratigraphy

[7] The PRAD1.2 borehole was drilled on the upper continental slope south of the MAD (42°40′34.7″N, 14°46′13.5″E) in 185.5 m water depth (Figure 2). The borehole provided a continuous core of 71.2 m with a 99.96% recovery, covering a time interval of about 400 kyr [*Piva et al.*, 2008a, 2008b]. The stratigraphy of PRAD1.2 integrates results from ecobiostratigraphic analyses of planktic and benthic foraminifera, $\delta^{18}O$ records, magnetic parameters and tephrochronology, lithology and XRF data (see Figure 4).

[8] The analysis of high-resolution seismic profiles shows that the borehole penetrates a uniform succession consisting of subparallel reflectors, with a slight plunge toward the NE (Figures 2 and 3). The sampled stratigraphic units represent the distal expression of the depositional sequences that are discernible on the shelf [*Ridente et al.*, 2008]. The stratigraphic units, starting from the youngest, are (1) highstand (HST) and transgressive (TST) deposits of the last glacial cycle, (2) lowstand progradation deposit (LST) from the Po River delta, and (3) four late Pleistocene regressive depositional sequences each recording a sea level cycle at the 100 kyr scale [*Piva et al.*, 2008a; *Ridente et al.*, 2008].

[9] The depositional pattern of each sequence upslope of the borehole may be divided into two main seismic units: (1) uniform and subparallel seismic reflectors, connected to the progradational units deposited during interglacial intervals of Marine Isotope Stage (MIS) 5, 7, and 9 [*Martinson et al.*, 1987], forming the bulk of sequences 1–3, and (2) onlapping units formed by landward converging seismic reflectors that pinch-out toward the shelf edge, corresponding to the lowstand cold intervals (Figure 3). These latter units are separated by the distal correlative of shelf erosional surfaces ES1 to ES3 that split seaward into a sequence boundary (SB) and a transgressive surface (Ts). Instead, surface ES4, as well the deepest unconformity ES5 (not reached by the borehole), maintains an erosional character on the upper slope and at the borehole site [*Ridente et al.*, 2008].

[10] The stratigraphic units recovered are mainly composed of marine mud with thin silty layers which, in some cases, correspond to pyroclastic deposits. Sand layers occur only around 58 m below the seafloor (mbsf) and correspond to the shallowest depositional environment encountered by the borehole (Figure 4).

3. Methods

[11] The reconstruction of the tectonic history of the central Adriatic continental margin follows the backstripping method, first attempted by *Sleep* [1971], and then extensively

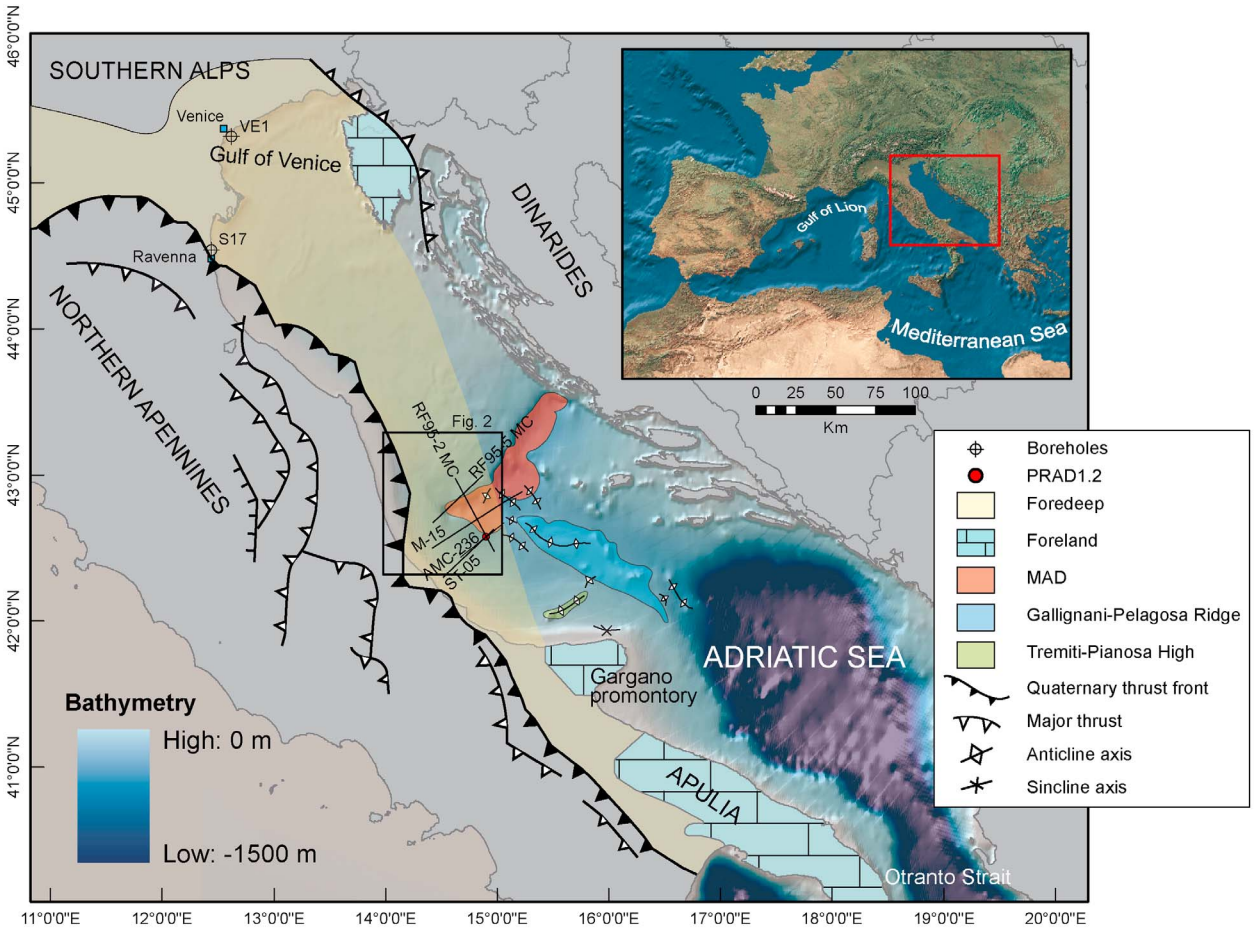

Figure 1. Bathymetry of the Adriatic Sea reporting the main structural elements of the central Apennine chain and surrounding foredeep-foreland systems (modified from *Patacca and Scandone* [2004]). Track lines refer to the seismic profiles shown in Figures 2, 4, and 12; circles denote the location of the PRAD1.2 borehole and two additional boreholes along the north Adriatic shoreline: VE1 and S17. Black box refers to the location in Figure 2. MAD, Mid Adriatic Deep.

discussed by *Watts and Ryan* [1976] and by *Steckler and Watts* [1978]. The backstripping method is a numerical stratigraphic technique with the aim of investigating the geologic history of a sedimentary basin, taking into account compaction processes of the sediment column, variations in paleowater depth and sea level changes as well as isostatic rebound effects. Backstripping is successfully applied over long timescales (millions of years); when such long intervals are taken into account, only few assumptions are necessary and the impact of errors on the reconstruction of paleowater depth is reduced; this is particularly the case when referring to long boreholes encompassing shallow water environments [*Angevine et al.*, 1990]. In contrast, applying the backstripping method to short boreholes proves more problematic, in particular when referring to recent time intervals (i.e., the last few hundreds of thousands of years), dominated by high-magnitude and high-frequency sea level oscillations which imply a more problematic reconstruction of the paleowater depth and a poorer definition of the lithospheric response to rapid load changes.

[12] Following *Angevine et al.* [1990], the borehole PRAD1.2 was divided into 16 units, and the position of each stratigraphic horizon was restored to its depth at the time of deposition on the basis of compaction corrections (see Appendix A). The units are defined on the basis of the major isotopic shifts and the available geochronological control points (see *Piva et al.* [2008a] for a detailed isotopic stratigraphy and chronology of PRAD1.2). These units, named "U" and "T," are numbered referring, broadly, to the corresponding Marine Isotopic Stages; in particular, "T" units cover periods of high rate of sea level rise (see Figure 4 and Table 1).

[13] To construct the total subsidence curve it is necessary to take into account the paleowater depth of the stratigraphic horizons and the global sea level changes. As stated by *Allen and Allen* [1990], referring to sea level changes from first- to third-order cycles, the latter correction can be avoided because of the large error bars of the eustatic curves and their uncertain origin (tectonic versus ice volume). In the case of PRAD1.2 this correction is possible and necessary, because sea level during the interval examined is the main driver for any change in water depth. Furthermore, the borehole was retrieved beyond the shelf edge and therefore the determination of paleowater depth is more uncertain for

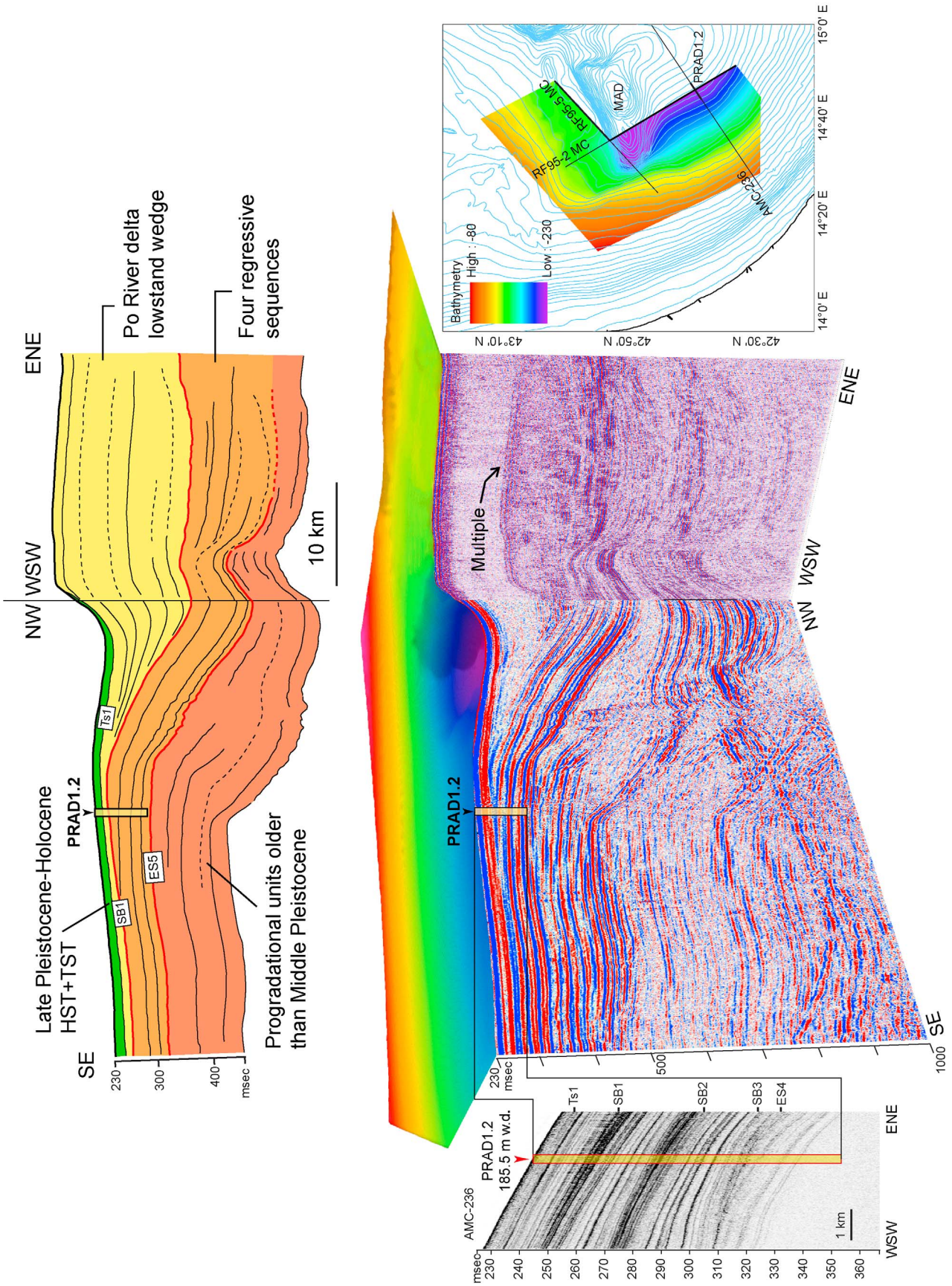
NW WSW
ENE
Po River delta
lowstand wedge
Four regressive
sequences
10 km
Late Pleistocene-Holocene
HST+TST
PRAD1.2
Ts1
SB1
ES5
Progradational units older
than Middle Pleistocene
SE
230
300
400
msec
Bathymetry
High : -80
Low : -230
RF95-2 MC
RF95-5 MC
MAD
PRAD1.2
AMC-236
14°0' E
14°20' E
14°40' E
15°0' E
42°30' N
42°50' N
43°10' N
Multiple
PRAD1.2
NW WSW
ENE
SE
230
msec
500
1000
AMC-236
PRAD1.2
185.5 m w.d.
Ts1
SB1
SB2
SB3
ES4
1 km
WSW
ENE
msec
230
240
250
260
270
280
290
300
310
320
330
340
350
360

Figure 2

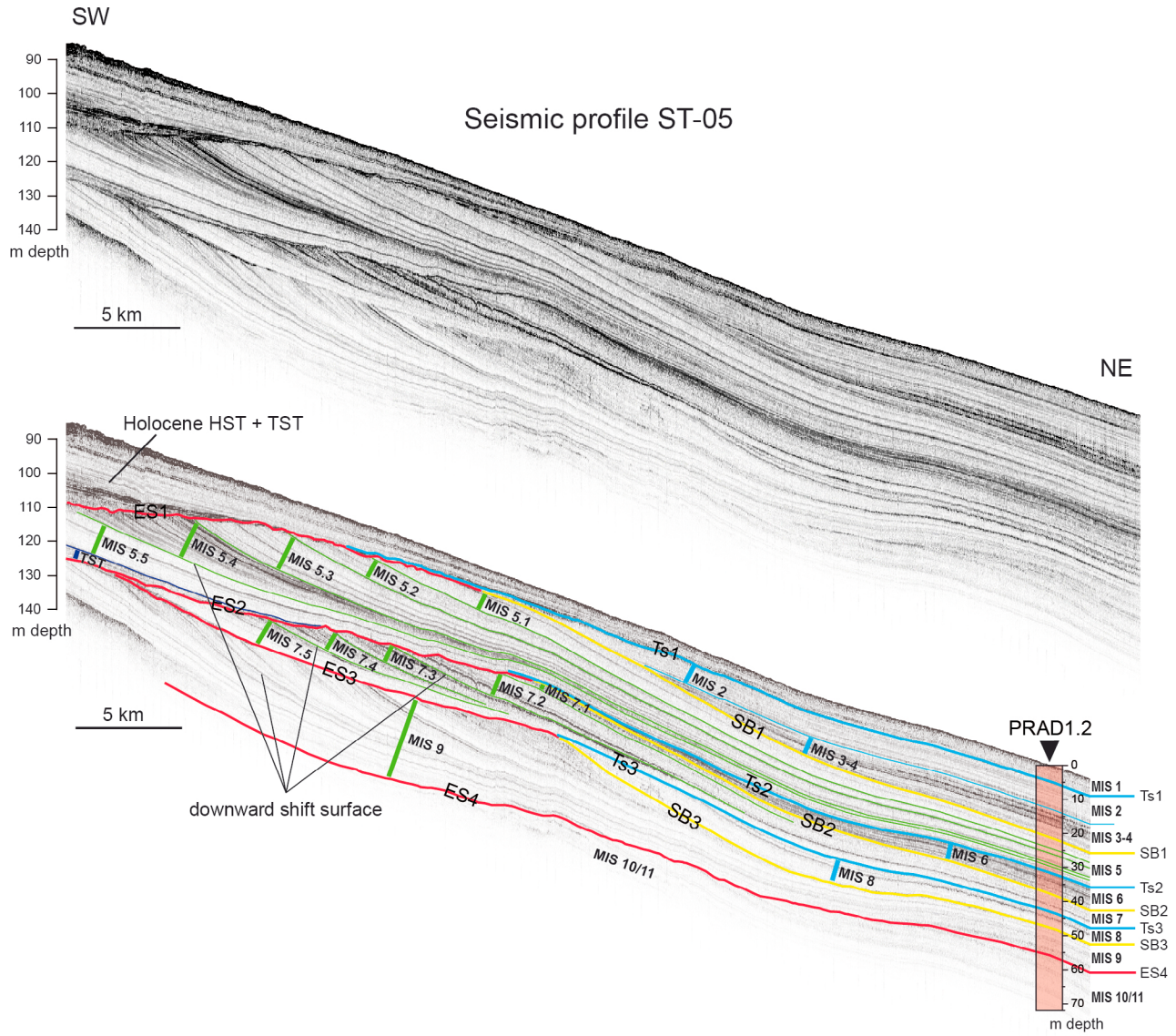

Figure 3. (top) High-resolution chirp sonar profile crossing the site of the borehole PRAD1.2. (bottom) Shelf-slope correlation of the depositional sequences across the site of the borehole PRAD1.2. Highstand, lowstand, and falling stage systems' tracts can be distinguished on the basis of their reflector geometry and biostratigraphic data [see *Piva et al.*, 2008a]. Highstand and falling sea level sequences can be correlated across the margin (green lines), while lowstand deposits remain confined to an upper slope position (blue lines). The unconformities (ES) at the base of each depositional sequence show an erosional character on the shelf, while seaward of the shelf edge they split into a sequence boundary (SB) below and a transgressive surface (Ts) above.

some stratigraphic intervals where benthic faunas are less diagnostic.

[14] All the parameters introduced above are affected by errors. The first source of error can be related to the isostatic balance model used for the backstripping procedure. Following the results of *Steckler and Watts* [1978], showing no much difference between local compensation and a more complex flexural model, we decided to use an Airy isostatic model. This approach is preferred also considering the small load of the sedimentary succession analyzed and the poor definition of the equivalent elastic thickness in the central Adriatic region.

Figure 2. Stratigraphy of the central Adriatic basin along a NNW–SSE section based on the interpretation of high-resolution multichannel seismic profiles RF95-2MC and RF95-5MC. On the left side is the high-resolution seismic stratigraphy at PRAD1.2 borehole (seismic line AMC-236); the sequence boundaries are labeled SB1–SB3 and ES4 from top to bottom. HST, highstand; TST, transgressive; m w.d., meters water depth.

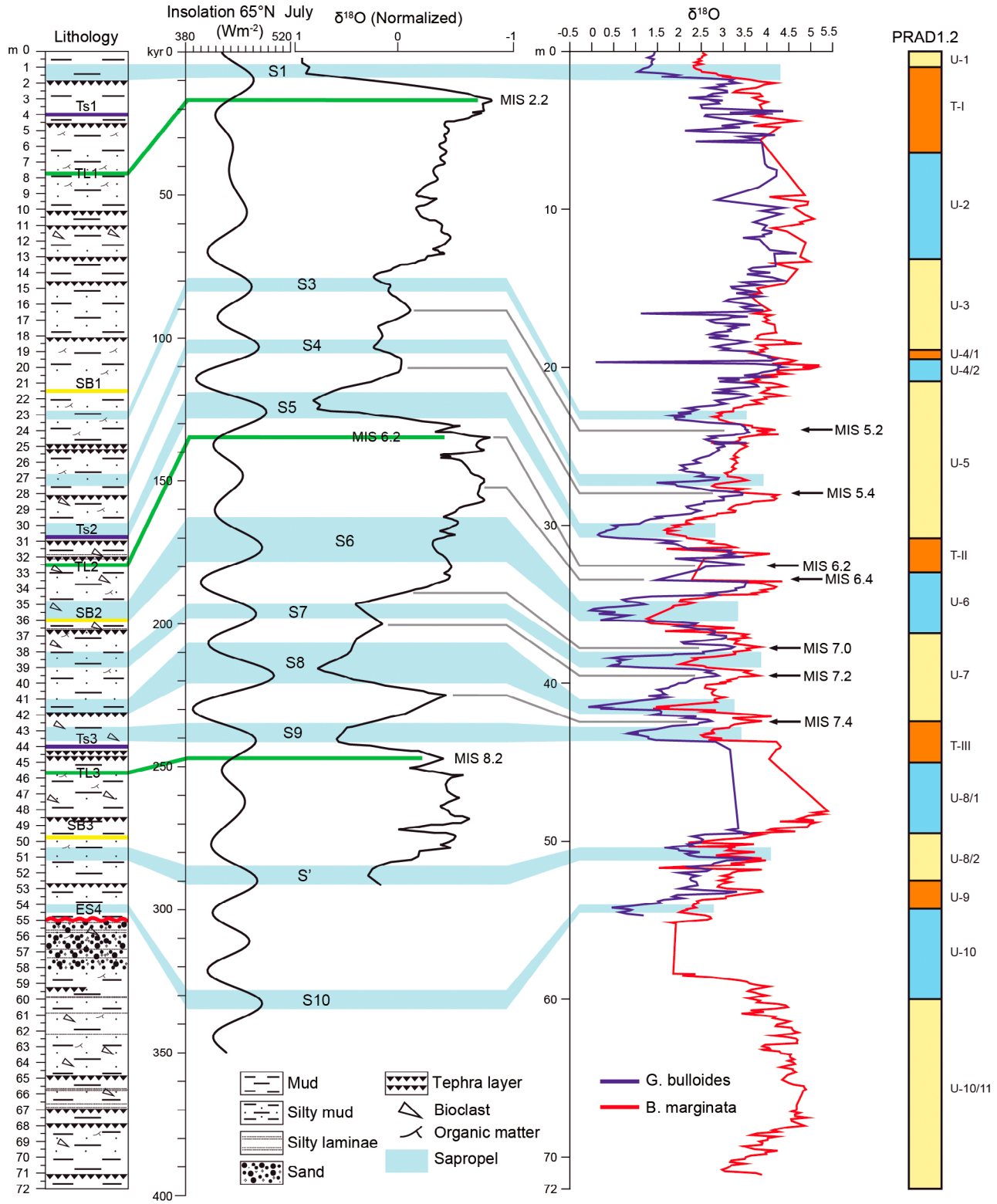
Lithology
Insolation 65°N July (Wm-2)
δ18O (Normalized)
δ18O
PRAD1.2
kyr
m
Ts1
TL1
SB1
Ts2
TL2
SB2
Ts3
TL3
SB3
ES4
S1
S3
S4
S5
S6
S7
S8
S9
S10
S'
MIS 2.2
MIS 6.2
MIS 8.2
MIS 5.2
MIS 5.4
MIS 6.2
MIS 6.4
MIS 7.0
MIS 7.2
MIS 7.4
U-1
T-I
U-2
U-3
U-4/1
U-4/2
U-5
T-II
U-6
U-7
T-III
U-8/1
U-8/2
U-9
U-10
U-10/11
Mud
Silty mud
Silty laminae
Sand
Tephra layer
Bioclast
Organic matter
Sapropel
G. bulloides
B. marginata

Figure 4

Table 1. Borehole PRAD1.2 Subdivided Into 16 Units on the Basis of the Control Points Available, to Perform the Decompaction Calculation and the Backstripping Procedure[a]

Unit Name	Base Depth (m)	Age (kyr)	Thickness (m)	Porosity (%)	Sediment Grain Density (kg/m^3)
U-1	1	7.2 (±1)[1]	1	71	1520
T-I	6.4	17.5 (±0.8)[1]	5.4	57.3	1750
U-2	13.2	27.3 (±0.8)[1]	6.8	51.6	1820
U-3	18.9	57.5 (±1.5)[2]	5.7	53.5	1820
U-4/1	19.5	61 (±1.8)[2]	0.6	51.4	1820
U-4/2	20.8	68 (±2)[2]	1.3	53.6	1820
U-5	30.7	125 (±3)[3]	9.9	53.7	1820
T-II	33	143 (±5)[4]	2.3	48.6	1850
U-6	36.8	184 (±3)[3]	3.8	52.3	1910
U-7	42.4	225 (±5)[4]	5.6	48.1	1900
T-III	45.1	248 (±4)[5]	2.7	44.6	1890
U-8/1	49.5	263 (±3)[3]	4.4	48	1900
U-8/2	52.5	315 (±3)[3]	3	53.2	1950
U-9	54.2	331 (±3)[3]	1.7	43.9	1950
U-10	60	340 (±5)[6]	5.8	42	1900
U-10/11	71.2	365 (±5)[6]	11.2	47.8	1850

[a]For each unit, Table 1 gives the depth of the bottom and the age, the thickness, the average porosity, and the sediment grain density values. Porosity was obtained indirectly by grain density values from multisensor core logger. Error bars are as follows: 1, from *Piva et al.* [2008a]; 2, from *Meese et al.* [1997]; 3, from *Lourens* [2004]; 4, from *Martinson et al.* [1987]; 5, from *Lisiecki and Raymo* [2005]; 6, from *Bassinot et al.* [1994]. T, isotopic termination. See Figure 4.

[15] The errors in PRAD1.2 age model, based on a combination of control points derived from different techniques, depend on the dating method [*Piva et al.*, 2008a]: midpoint of isotopic terminations (II and III) (error ± 4 kyr [*Lisiecki and Raymo*, 2005]) and isotopic wiggle matching with other records (error ± 5 kyr [*Martinson et al.*, 1987; *Bassinot et al.*, 1994]), biostratigraphic events (variable timescale and errors [see *Piva et al.*, 2008a]), recognition of a well-dated polarity inversion of the magnetic field [*Laj et al.*, 2006], correlation to sapropel-based stratigraphy [*Lourens*, 2004], and 6 ^{14}C AMS calibrated ages [*Piva et al.*, 2008a].

[16] Errors introduced in the decompaction process are more difficult to assess because their calculation involves iterative solutions of the nonlinear porosity-depth equation of *Athy* [1930], whereby the error at any particular depth is affected also by the error of the above section [*Waltham et al.*, 2000]. In the literature the main source of error can be identified in the decompaction parameters (initial porosity, porosity coefficient and density; see Appendix A for details), often based on empirical relations. In the case of PRAD1.2 this source of error can be neglected mainly because the porosity and density values are obtained by a sonic log and the borehole is only 71.2 m long.

[17] In the PRAD1.2 the main source of error can be identified in the paleowater depth reconstructions and in the definition of eustatic curves. Even if the latter can be avoided considering the most recent published sea level curves [*Lea et al.*, 2002], remain the problem regarding the correct evaluation of the water depth of past depositional environments. In this case, paleowater depth is obtained following the relation showed by *Van der Zwaan et al.* [1990], while error bars are given on the base of benthonic foraminifera assemblages (for a detailed description, see Appendix B).

[18] Finally, the values obtained are compared with the results of an independent approach based on the identification of lowstand paleoshorelines (over the last 340 kyr BP) on high-resolution CHIRP-sonar profiles acquired over the past 15 years by CNR-ISMAR. This technique, successfully applied in other continental margins (e.g., Gulf of Lion [*Rabineau et al.*, 2006]), gives the possibility of a detailed evaluation of the subsidence rates, with a better spatial and temporal resolution, and a better definition of uncertainties and error bars associated.

4. Results

4.1. Backstripping of PRAD1.2

[19] On the basis of the high-resolution stratigraphy and paleoenvironmental reconstructions showed by *Piva et al.* [2008a, 2008b] and *Ridente et al.* [2008], the central Adriatic margin is investigated applying the geohistory analysis to the borehole PRAD1.2, in order to quantify the total subsidence and the contribution of the sediment load and tectonic driving forces.

[20] The *first step* of the geohistory analysis was to subdivide the stratigraphic succession into elementary units, each characterized by specific porosity and grain density values; the borehole PRAD1.2 was subdivided into 16 stratigraphic

Figure 4. (left) Lithostratigraphy of PRAD1.2 (modified from *Ridente et al.* [2008]). The PRAD1.2 borehole encompasses the distal part of the last four late Quaternary depositional sequences. The borehole is characterized by an overall fine-grained lithology, punctuated by coarser (silty or sandy) layers, mainly in the lower part of the core to the ES4 surface. Note that the interval between 55 and 58 m is characterized by a thick sandy unit with reworked microfauna and an erosional base. Yellow lines refer to sequence boundaries (SB); blue lines refer to transgressive surfaces (Ts); the red line refers to erosional surface ES4; and green lines refer to time lines (TL) corresponding to the cold isotopic events 2.2, 6.2, and 8.2 (see Tables 4 and 5). (middle) Sapropel and isotopic (δ^{18}O) stratigraphy of PRAD1.2 with the main isotopic events [*Piva et al.*, 2008a]. Insolation curve 65°N refers to *Berger and Loutre* [1991]; normalized δ^{18}O curve refers to *Martinson et al.* [1987]. (right) Subdivision of PRAD1.2 for decompaction and backstripping calculations.

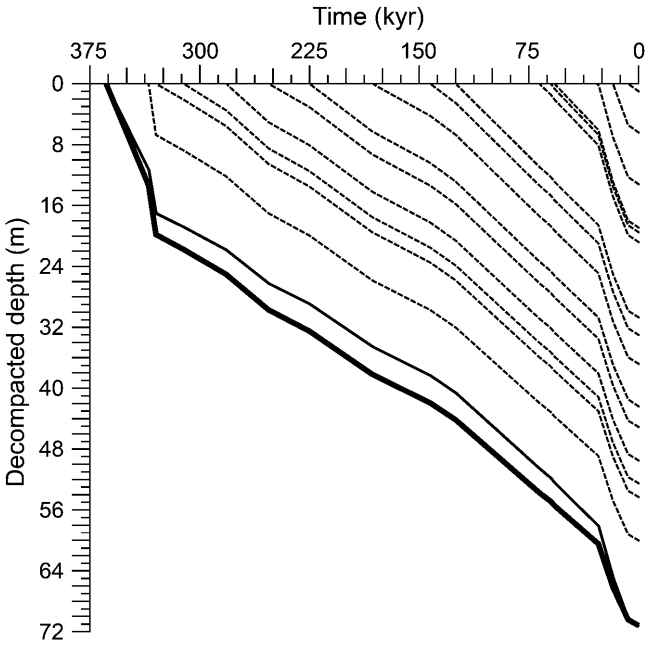

Figure 5. Decompaction plot obtained from Table A1. Each dashed line shows the depth of the borehole at each time step. The thick line is the total decompacted subsidence curve; the thin line is the present-day borehole without decompaction.

units (see Table 1 and Figure 4). In order to calculate the thickness of each individual unit at the time of its deposition, two main assumptions are necessary: (1) any change in volume of a sediment unit in the burial process is due to a change only in porosity and not in the grain size, and (2) sediment is fully compacted at the time of sampling. Following the calculations reported in Appendix A, the decompacted subsidence history of the borehole could be plotted in a diagram of depth versus age where the bottom bold line represents the subsidence at the base of the borehole (Figure 5). At this point it is also possible to calculate the sedimentation rate for each decompacted unit in mm/yr (Table 2). Figure 6 shows that the sedimentation rate is almost constant at 0.15 mm/yr, even if there are two short intervals, centered around MIS 2 and MIS 10, that appear to reach 0.72 and 0.75 mm/yr, respectively.

Table 2. Sedimentation Rates Obtained From Decompacted Thickness

Unit Name	Decompacted Thickness (mm)	Time Interval (kyr)	Sedimentation Rate (mm/yr)
U-1	1000	7.2 (±1)	0.14 (±0.02)
T-I	5427	10.5 (±0.8)	0.52 (±0.04)
U-2	7015	9.8 (±0.8)	0.72 (±0.06)
U-3	6076	30.2 (±1.5)	0.20 (±0.01)
U-4/1	656	3.5 (±1.8)	0.19 (±0.09)
U-4/2	1429	7 (±2)	0.20 (±0.06)
U-5	10895	57 (±3)	0.19 (±0.01)
T-II	2532	18 (±5)	0.14 (±0.04)
U-6	4215	41 (±3)	0.10 (±0.01)
U-7	6277	41 (±5)	0.15 (±0.02)
T-III	3079	23 (±4)	0.13 (±0.07)
U-8/1	5056	15 (±3)	0.34 (±0.02)
U-8/2	3492	52 (±3)	0.07 (±0.004)
U-9	2101	16 (±3)	0.13 (±0.02)
U-10	6720	9 (±5)	0.75 (±0.4)
U-10/11	13368	25 (±5)	0.54 (±0.1)

[21] In order to obtain the total subsidence curve it is necessary to introduce the paleowater depth of each horizon and consider the global sea level oscillation, representing the datum from which the water depths are then calculated. The total subsidence curve (see Figure 5, bottom line) takes into account all the following contributions: sediment load, tectonic load, thermal cooling (if applicable) and water load. The backstripping procedure allows one to quantify the contribution of each parameter by solving the following equations:

$$Z_i = S^* \left(\frac{\rho_a - \overline{\rho}_b}{\rho_a - \rho_w} \right) + W_{d_i} - \Delta_{sl_i}, \quad (1)$$

$$S^* = \sum_{j=1}^{i} T_j^*, \quad (2)$$

where Z_i is the tectonic subsidence ($[Z_i]$ = m), S^* is the total thickness of the decompacted sedimentary column at the time t ($[S^*]$ = m), ρ_a is the density of the underlying material, under the sediment section ($[\rho_a] = 3330$ kg/m^3), $\overline{\rho}_b$ is the bulk

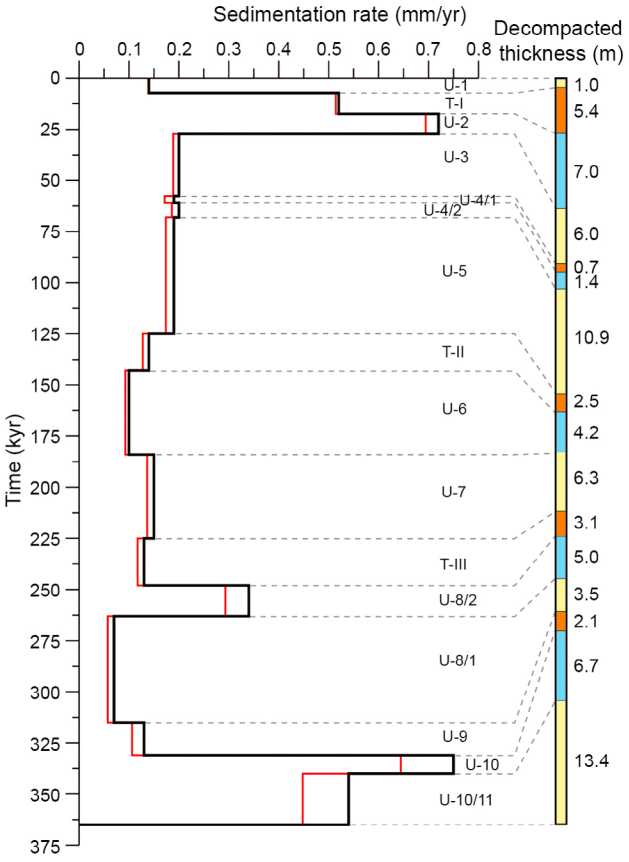

Figure 6. Undecompacted (red line) and decompacted (black line) sedimentation rate for borehole PRAD1.2, obtained from Table 2. The average sedimentation rate is about 0.15 mm/yr, even if two peaks are present at 20 kyr (0.7 mm/yr) and 340 kyr (0.75 mm/yr). On the right is the decompacted thickness of the 16 units of the borehole.

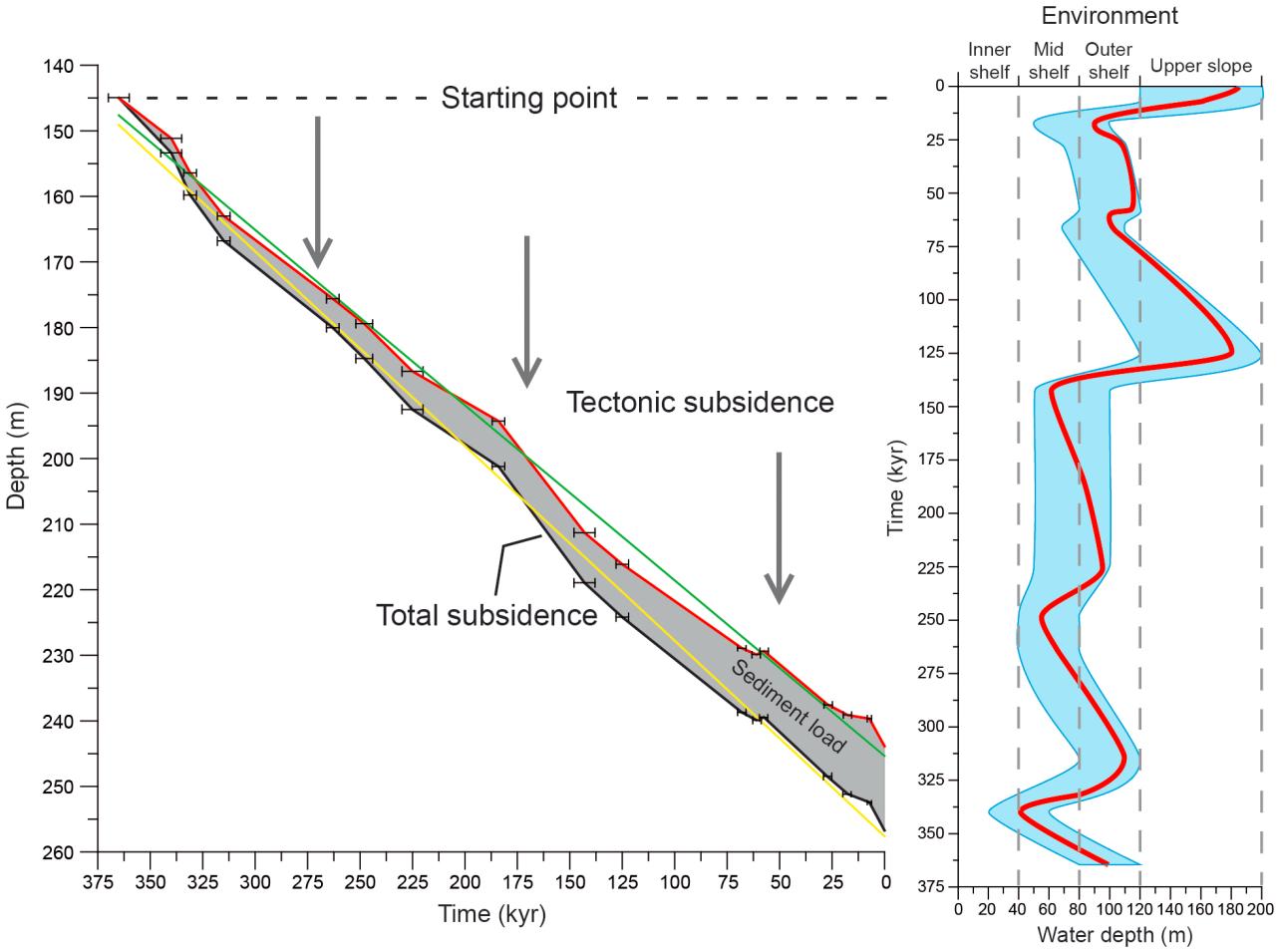

Figure 7. Backstripping diagram of borehole PRAD1.2. The black line represents the total subsidence curve (see also Figure 5), the red line is the tectonic subsidence, and the gray area is the sediment load. The two fitting curves are the total subsidence (yellow line: about 0.3 mm/yr) and the tectonic subsidence (green line: about 0.27 mm/yr). The diagram on the right represents the paleowater depths: the red line is obtained following the theory of *Van der Zwaan et al.* [1990], while the blue envelope represents the environment obtained from the foraminifera associations (see Table 3 for a detailed description of each parameter).

density of the sedimentary column ($[\overline{\rho}_b]$ = kg/m^3), ρ_w is the density of salt water ($[\rho_w]$ = 1030 kg/m^3), W_{d_i} is the paleowater depth ($[W_{d_i}]$ = m), and Δ_{sl_i} is the sea level oscillations ($[\Delta_{sl_i}]$ = m).

[22] Equation (1) is still a simplified version of the backstripping equation, because no isostatic correction is introduced for changes in water load. This simplification derives from the evidence that the Airy correction for rapid changes in water load gives nonlinear results, meaning that lithospheric adjustment for rapid changes in surface load cannot be simplified by an Airy isostatic model. Figure 7 shows the results of the backstripping procedure and the paleowater depth values used for the calculation. In detail, the red line of the diagram on the right of Figure 7 shows the paleowater depth obtained following the approach defined by *Van der Zwaan et al*. [1990], while the blue envelope, representing the confidence interval of each values, is based on the modern (present-day) range of water depths of each living benthonic foraminifera assemblage (see Table 3 and Appendix B for details). The diagram on the left of Figure 7 represents the backstripping of PRAD1.2: the black line is the total subsidence curve that reflects all processes contributing to subsidence; the red line at the top portrays the tectonic subsidence alone. The interval between the two curves shows the subsidence due to the ~72 m of sediment load. Despite the large vertical error bars due to the uncertainties in paleowater reconstructions, it is possible to estimate the contribution of sediment load and tectonics by fitting the two curves with a linear regression. The result is that the total subsidence of the borehole PRAD1.2 is about 0.3 mm/yr (yellow line), and is mostly ascribed to tectonic driving forces (0.27 mm/yr, green line). Given the inevitable large spread of uncertainty we introduce an independent method to constrain the total subsidence by defining the relative depth of shorelines during the last four glacial lowstands.

4.2. Independent Subsidence Estimates From Dated Lowstand Shorelines

[23] An independent approach for the calculation of subsidence rates, commonly applied on other continental

Table 3. Parameters Necessary for the Backstripping Procedure

Unit Name	Unit Age[a] (kyr)	Decompacted Depth[b] (m)	Sea Level[c] (m)	Water Depth[d] (m)	Foraminifera Assemblages[e]	Environment[e]	Bathymetric Range[e] (m)
Present day	0.0	71.2	0	185.50	***B. dilatata***, ***C. laevigata carinata***, *B. marginata*, *C. pachyderma*, *T. angulosa*, *U. mediterranea*, *U. peregrina*, *G. subglobosa*, *H. balthica*, *P. ariminensis*	Upper slope	120–200
U-1	7.2 (±1)[1]	70.415	−20.0	162.0	***B. dilatata***, ***C. laevigata carinata***, *B. marginata*, *G. subglobosa*, *H. balthica*, *T. angulosa*, *U. peregrina*, *C. pachyderma*, *M. barleeanum*	Upper slope	120–200
T-I	17.5 (±0.8)[1]	66.162	−95.0	90.0	***S. sellii***, ***N. depressulum***, ***E. crispum***, ***E. decipiens***, *G. laevigata*, *M. rotunda*, *B. marginata*, *Q. seminulum*	Mid-Outer shelf	50–100
U-2	27.3 (±0.8)[1]	60.461	−80.0	108.0	***C. laevigata carinata***, ***E. crispum***, *Q. seminulum*, *E. decipiens*	Mid-Outer shelf	70–110
U-3	57.5 (±1.5)[2]	55.445	−70.0	114.0	***B. marginata***, ***H. balthica***, ***E. decipiens***, *E. crispum*, *G. subglobosa*, *N. depressulum*, *Q. seminulum*, *T. angulosa*, *U. mediterranea*, *U. peregrina*	Outer shelf	80–120
U-4/1	61 (±1.8)[2]	54.899	−85.0	100.0	***C. laevigata carinata***, ***H. balthica***, ***N. depressulum***, *E. crispum*, *E. decipiens*	Mid-Outer shelf	70–110
U-4/2	68 (±2)[2]	53.709	−80.0	105.0	***B. marginata***, ***C. laevigata carinata***, ***H. balthica***, *T. angulosa*, *E. decipiens*, *E. crispum*, *P. ariminensis*, *Q. seminulum*, *U. mediterranea*, *U. peregrina*	Mid-Outer shelf	70–110
U-5	125 (±3)[3]	44.173	0	180.0	***B. dilatata***, ***B. marginata***, ***C. laevigata carinata***, ***Globobulimina***, *C. oolina*, *B. costata*, *C. bradyi*, *C. pachiderma*, *G. praegeri*, *H. balthica*, *Q. seminulum*, *U. mediterranea*, *U. peregrina*	Sapropel equivalent (Upper slope)	120–200
T-II	143 (±5)[4]	41.94	−115.0	62.0	***I. islandica***, ***Trifarina* sp. 1**, ***E. articulatum***	Mid-Outer shelf	50–100
U-6	184 (±3)[3]	38.195	−80.0	83.0	***C. laevigata carinata***, ***E. crispum***, ***E. decipiens***, ***I. islandica***, *B. marginata*, *G. praegeri*, *G. subglobosa*, *P. ariminensis*, *Q. seminulum*, *Trifarina* sp1, *T. angulosa*	Mid-Outer shelf	50–100
U-7	225 (±5)[4]	32.521	−65.0	95.0	***B. marginata***, ***C. laevigata carinata***, *B. dilatata*, *C. pachyderma*, *E. crispum*, *E. decipiens*, *G. praegeri*, *I. islandica*	Mid-Outer shelf	50–100
T-III	248 (±4)[5]	29.716	−100.0	55.0	***I. islandica***, ***E. articulatum***, ***Nonion* sp. 1**, *N. depressulum*, *E. crispum*	Midshelf	40–80
U-8/1	263 (±3)[3]	25.043	−90.0	65.0	***C. laevigata carinata***, ***I. islandica***, *B. marginata*, *B. dilatata*, *E. crispum*, *E. decipiens*, *Nonion* sp. 1	Midshelf	40–80
U-8/2	315 (±3)[3]	21.783	−35.0	110.0	***B. dilatata***, ***B. marginata***, ***C. laevigata carinata***, *B. costata*, *E. crispum*, *E. decipiens*, *E. exigua*, *M. barleeanum*, *P. ariminensis*, *T. angulosa*, *U. peregrina*	Outer shelf	80–120
U-9	331 (±3)[3]	19.81	−60.0	80.0	***B. dilatata***, ***B. marginata***, ***C. laevigata carinata***, *G. subglobosa*	Mid-Outer shelf	50–100
U-10	340 (±5)[6]	13.368	−100.0	40.0	***B. marginata***, ***Nonion* sp. 1**, *E. decipiens*, *E. crispum*, *N. depressulum*	Inner-Mid shelf	20–60
U-10/11	365 (±5)[6]	0	−45.0	100.0	*B. marginata*, *C. laevigata carinata*, *E. crispum*, *E. decipiens*, *E. exigua*	Outer shelf	80–120

[a]For errors in ages, refer to Table 1.
[b]For a detailed description of decompaction procedure, see Appendix A and Table A1.
[c]Sea level values refer to *Lea et al.* [2002]; the average error on sea level estimates is about 20 m [*Lea et al.*, 2002].
[d]Paleowater depth values are obtained following the theory explained by *Van der Zwaan et al.* [1990].
[e]The environment and bathymetric range obtained analyzing the foraminifera associations [*Piva et al.*, 2008a, 2008b]: the taxa with the highest abundances (>10%) are in bold italics, the taxa with common abundance (5–10%) are in underlined italics, and the taxa with frequency of 1–5% are in italics (see also Appendix B).

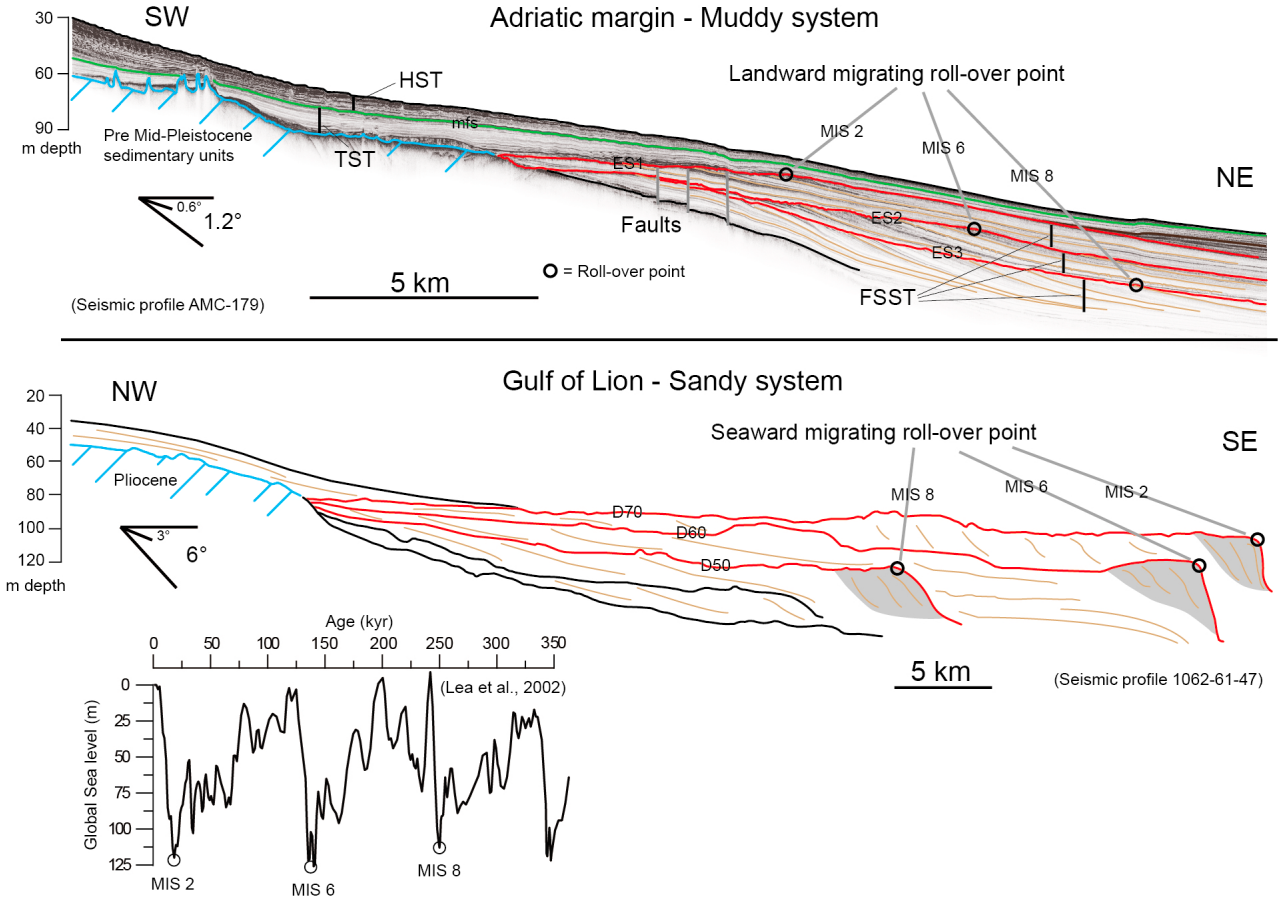

Figure 8. Comparison between the Adriatic active continental margin and the passive margin of the Gulf of Lion. (top) Line drawing along seismic profile AMC-179 (see also Figure 11). Circles represent the position of the lowstand shorelines, showing a backstepping configuration indicating that subsidence rate is greater than sediment supply. FSST, falling stage systems' tracts; mfs, maximum flooding surface. (bottom) Profile showing basinward tilt due to sedimentary load (modified from *Jouet et al.* [2006]). Progradation of the lowstand shorelines from MIS 8 to MIS 2 implies that subsidence rate is less than sediment supply. The greater subsidence of the Adriatic margin is marked by the landward shift of the landward pinch-outs of the sequences. Reference sea level curve is from *Lea et al.* [2002].

margins, is based on the identification of lowstand shoreline deposits of known age (e.g., in the Gulf of Lion [*Rabineau et al.*, 2006; *Skene et al.*, 1998]). These deposits can be identified also in the Adriatic margin from their diagnostic morphologies and internal reflector geometries on seismic profiles and their ages can then be assessed through their correlation with the stratigraphy derived from PRAD1.2 borehole.

[24] The key features to identify a drowned shoreline include (1) the rollover point between topset and foreset beds in clinoforms, although this feature can be found in water depths up to 20–30 m [*Vail et al.*, 1977; *Steckler*, 1999; *Cattaneo et al.*, 2003, 2007]; (2) the basinward limit of the lowstand subaerial erosion and/or its changes in dip and morphology; (3) the occurrence of thin packages of shingled reflectors converging and downlapping seaward; and (4) a change in seismic facies, typically characterized by higher amplitudes with respect to the surrounding seismic units (Figure 8 and Figure 9, bottom).

[25] The type of sediment delivered is an important factor controlling the formation of thick and detectable shoreline deposits. Unlike the Gulf of Lion and other Mediterranean margins characterized by coarser sediment, the Adriatic sequences are mainly pelitic. Sand-dominated systems are characterized by a well defined sedimentary prism with foreset beds dipping at high angles, typically of 3°–7° and a marked rollover point; in contrast, muddy systems are characterized by very low relief, and a shallower and less pronounced rollover point. In a first approximation, in the case of muddy systems the transition between an erosional unconformity and its correlative conformity can be considered to approximate a paleoshoreline. This assumption may lead to an error, up to several meters, because submarine erosion may extend further seaward and downward [*Thorne and Swift*, 1991].

[26] Paleoshorelines identified in this work are referred to changes in dip of the erosional surface often connected to thin reflector packages downlapping seaward. Since the Adriatic margin is characterized by a very low gradient shelf, a horizontal uncertainty of several hundreds of meters introduces an error of only a few meters in the paleoshoreline depth,

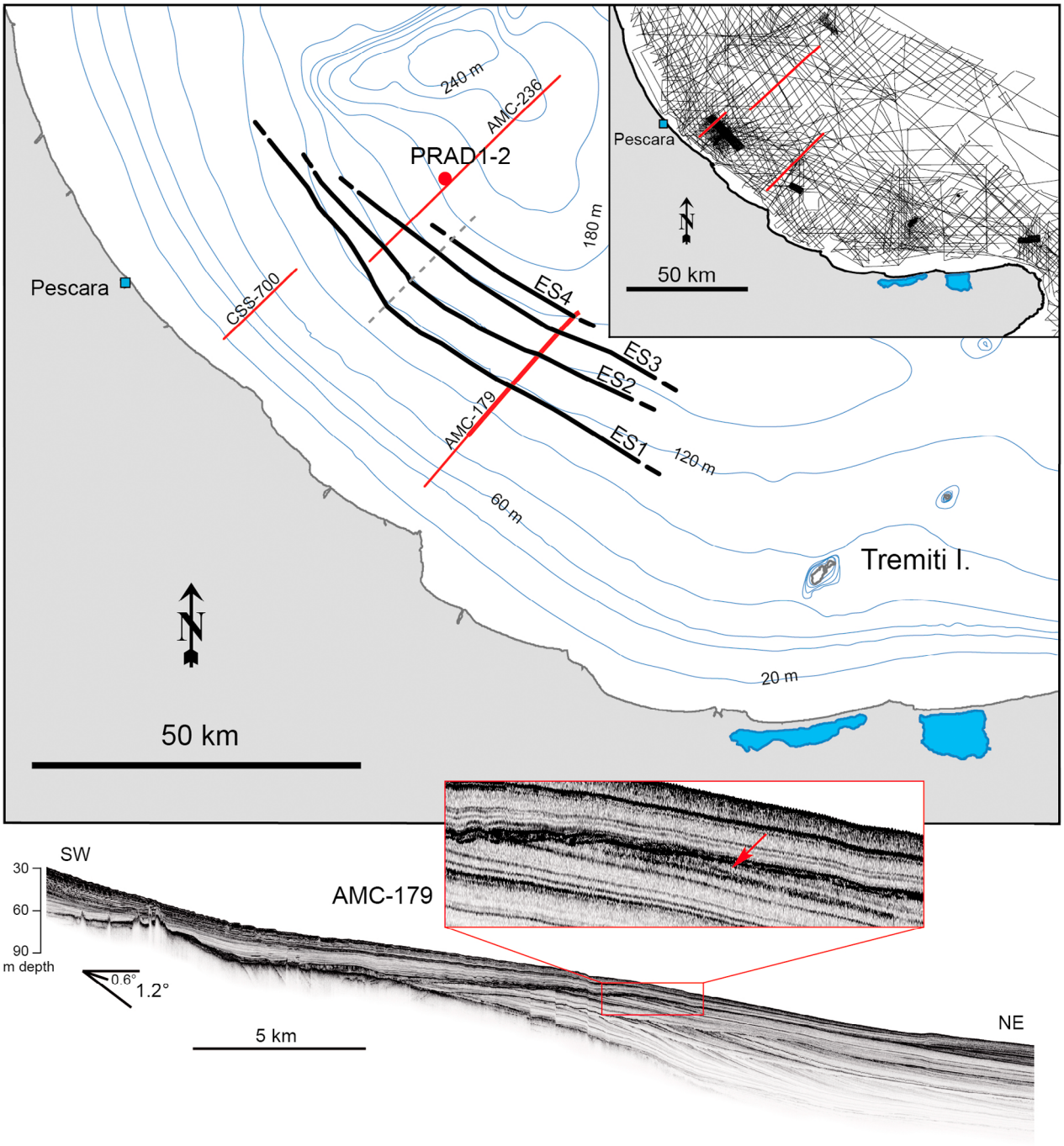

Figure 9. (top) Plane view of the lowstand shorelines (named ES1 to ES4, top down) showing a landward migration from MIS 10 (ES4) to MIS 2 (ES1). Note the basinward shift and the deepening of the lowstand shoreline ES1 and ES2 north of the dashed line (Table 4). This trend may reflect the configuration of the Eemian HST depocenter. (bottom) Detail of seismic profile AMC-179 showing a downlapping reflector interpreted as a possible shoreline deposit (red arrow).

maintaining a rather small range of uncertainty on the depth of each lowstand shoreline. The observed lowstand shorelines migrate landward from MIS 10 to MIS 2, following the backstepping pattern of the shelf perched wedge [*Trincardi and Correggiari*, 2000] (Figure 8).

[27] In plain view the lowstand shorelines become closer to each other proceeding in the NW direction, north of the dashed line in Figure 9, implying a relatively steeper margin or a faster seaward tilt during deposition. The depth of the shorelines associated to unconformities ES1–ES4 can be calculated by subdividing the margin in two areas, north and south of the dashed line in Figure 9, and averaging the values obtained analyzing the seismic profiles for each area (Table 4). To estimate the subsidence rate for each

Table 4. Depth of the Basinward Limits of the Glacial Lowstand Shorelines During the Cold Isotopic Events 2.2, 6.2, 8.2, and 10.2[a]

				North			South		
Shoreline	Age (kyr)	MIS	Eustatic Fall (m)	Average Depth (m)	Corrected Depth (m)	Subsidence Rate (mm/yr)	Average Depth (m)	Corrected Depth (m)	Subsidence Rate (mm/yr)
ES1	19 (±1.3)[4]	2.2	118 (±2)[7]	130.7 (±1.5)	12.7 (±3.5)	0.67 (±0.23)	122.1 (±0.5)	4.1 (±2.5)	0.22 (±0.16)
ES2	135 (±4.2)[4]	6.2	127 (±3)[8,9]	165.3 (±1.2)	38.3 (±4.2)	0.28 (±0.04)	154.6 (±1.1)	27.6 (±4.1)	0.2 (±0.04)
ES3	250 (±5)[6]	8.2	120 (±8)[10]	189.8 (±1.3)	69.8 (±9.3)	0.28 (±0.04)	186.9 (±2)	66.9 (±10)	0.27 (±0.05)
ES4	335 (±5)[6]	10.2	128 (±6)[10]				218.9 (±2.1)	90.9 (±8.1)	0.27 (±0.03)

[a]Subsidence rates derived by taking into account sea level falls during glacial periods following the results of different authors in the literature. The depth of each lowstand shoreline is obtained by dividing the area of interest in two sectors (north and south of the dashed line in Figure 9) and averaging the values obtained from high-resolution seismic profiles. Error bars in age are as follows: 4, from *Martinson et al.* [1987]; 6, from *Bassinot et al.* [1994]. Error bars in sea level are as follows: 7, from *Bard et al.* [1990]; 8, from *Chappell and Shackleton* [1986]; 9, from *Shackleton* [1987]; 10, from *Rohling et al.* [1998]. Errors in average depth take into account uncertainties in horizontal position and in vertical resolution of the seismic lines.

sequence, the depth of each shoreline needs to be corrected for the eustatic sea level fall; this can be done by introducing different values for each eustatic cycle [*Bard et al.*, 1990; *Chappell and Shackleton*, 1986; *Rohling et al.*, 1998; *Shackleton*, 1987; *Lea et al.*, 2002]. Table 4 shows that the western side of the Adriatic margin is subsiding at 0.3 ± 0.08 mm/yr, with small but significant changes in subsidence rate in time and even in space, higher in the northern area. Figure 10 represents the subsidence trends detected from the depths at which the lowstand shorelines are encountered for each glacial interval. Note that the lowstand shorelines for glacial intervals between MIS 2 and MIS 10 fit a linear regression implying a constant subsidence over the last ~400 kyr of about 0.3 mm/yr.

[28] By using different values for the subsidence rate, taking into account the sediment supply corrected with an Airy isostatic compensation and by introducing the sea level fall for each glacial period, it is possible to extrapolate the paleowater depth at the peak of MIS 2.2, 6.2, 8.2 and 10.2 lowstands in the borehole PRAD1.2 (Table 5) and to compare the results with the paleowater depth reconstructions obtained by foraminifera assemblages.

[29] In detail, at 54.4 mbsf, corresponding to the top of MIS 10.2, seismic profiles show the erosional surface ES4 (Figures 2 and 4). This surface was generated by submarine erosion in water depth less than 20 m, as shown in Table 5 and confirmed by the lithological and paleontological data. One of the reflectors truncated by ES4 corresponds to a sharp surface at 58 mbsf in PRAD1.2 marking the base of a coarser-grained unit that likely indicates wave reworking in an inner shelf to shoreface environment. Moreover, in the interval between 55 and 58 m, abundant benthic microfauna indicates a very proximal inner shelf assemblage, with dominance of *Ammonia perlucida*, *Islandiella islandica*,

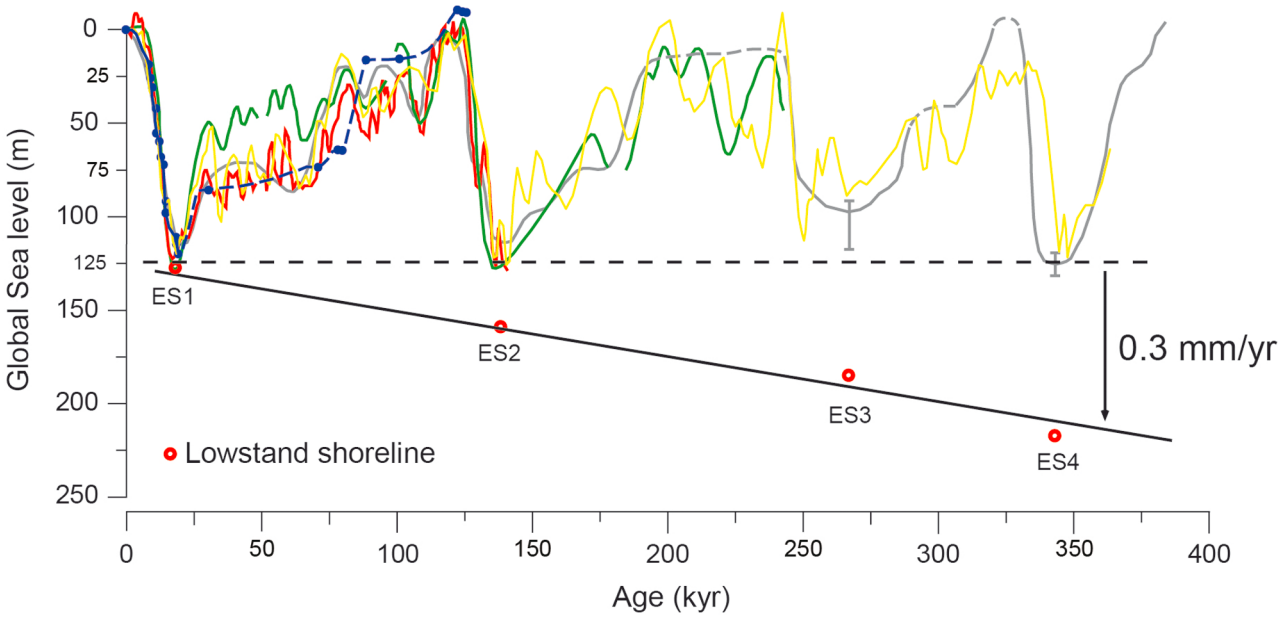

Figure 10. Present-day burial depths of paleoshorelines during major eustatic lowstands referred to isotopic stages from MIS 2 to MIS 10. The most commonly adopted eustatic curves help constrain the position of each successive lowstand shoreline: blue line is from *Bard et al.* [1990], points refer to U-Th ages, red line is from *Shackleton* [1987], green line is from *Chappell and Shackleton* [1986], gray line is from *Rohling et al.* [1998], and yellow line is from *Lea et al.* [2002]. Note that a simple regression fits the values, implying a quasi-steady subsidence rate during the last ~400 kyr.

Table 5. Paleowater Depth at the Site of PRAD1.2 During the Main Glacial Lowstands, TL1 to TL3 and ES4 (from MIS 2.2 to MIS 10.2)[a]

Boundary in PRAD1.2	Age (kyr)	MIS	Depth in PRAD1.2 (m)	Corrected Depth Airy (m)	Present-day Wd Correction (m)	Eustatic Fall (m)	Corrected Depth Eustatic Fall (m)	Subsidence Rate (mm/yr)	Subsidence Correction (m)	Paleowater Depth (m)	Foraminifera Assemblages	Environment	Bathymetric Range (m)
TL1	19 (±1.3)[4]	2.2	7.7	6.3	191.8	118 (±2)[7]	73.8 (±2)	0.45 (±0.23)	8.6 (±5)	65.2 (±7)	***C. laevigata carinata***, ***E. decipiens***, *N. depressulum*, *E. crispum*, *M. rotunda*, *S. sellii*, *G. laevigata*, *B. marginata*, *Q. seminulum*	Midshelf	40–80
TL2	135 (±4.2)[4]	6.2	32.5	26.6	212.1	127 (±3)[8,9]	85.1 (±3)	0.24 (±0.04)	32.4 (±6.4)	52.7 (±9.4)	***I. islandica***, ***Trifarina* sp1**, ***E. articulatum***, ***Nonion sp***	Midshelf	40–80
TL3	250 (±5)[6]	8.2	45.6	37.3	222.8	120 (±8)[10]	102.8 (±8)	0.27 (±0.05)	67.5 (±13.9)	35.3 (±21.9)	***I. islandica***, ***E. articulatum***, ***Nonion* sp. 1**, *N. depressulum*, *E. crispum*	Mid-Inner shelf	30–60
ES4	335 (±5)[6]	10.2	55	44.9	230.4	128 (±6)[10]	102.4 (±6)	0.27 (±0.03)	90.5 (±11.4)	11.9 (±17.4)	***I. islandica***, ***A. perlucida***, ***E. articulatum***, ***Nonion* sp. 1**, *N. depressulum*, *E. decipiens*	Inner-Mid shelf	10–30

[a]See also Figure 4. The values are obtained taking into account (1) present-day depth in core of the sequence boundaries and Airy correction for sediment unload, (2) present-day water depth (Wd) of 185.5 m, (3) sea level fall during lowstands from different eustatic curves (see Table 4 for references), and (4) reconstructed depth for different values of subsidence rate. The bathymetric range column shows the paleowater depth obtained from the foraminifera associations (see Table 3 and Appendix B).

Elphidium articulatum, and *Nonion pauciloculum* [*Piva et al.*, 2008a, 2008b].

[30] In MIS 8.2, *Piva et al.* [2008b] report a benthic assemblage dominated by *I. islandica* and *E. articulatum*. The absence of the inner shelf species *A. perlucida* (bathymetric range less then 30 m, according the local zonation reported by *Morigi et al.* [2005]) suggests a minor riverine influence along with a possible relatively deeper environment (midshelf). The calculation using a subsidence rate of 0.27 ± 0.05 mm/yr gives for MIS 8.2 a paleowater depth of about 40 m.

[31] MIS 6.2 is richer in planktic assemblages and characterized by benthic species typical of the midshelf to inner shelf environment. During the last glacial period, MIS 2.2, the PRAD1.2 borehole reached its maximum water depth as confirmed by the foraminifera assemblages, typical of a midshelf environment [*Piva et al.*, 2008b], and by the 65 m water depth calculated as above.

5. Discussion

5.1. Subsidence Rates in the Central Adriatic

[32] PRAD1.2 borehole is the only sedimentary record in the central Adriatic Sea encompassing the last ~400 kyr with a continuous core recovery. The lithological and paleontological information obtained [*Piva et al.*, 2008a, 2008b; *Ridente et al.*, 2008], correlated with a dense grid of seismic lines, made it possible to reconstruct the evolution of the margin and estimate the subsidence rate following an analytical model integrated by sedimenthological and seismostratigraphic evidences. The calculated subsidence rates of 0.3 mm/yr from PRAD1.2 borehole are consistent with the Facies and paleontological data, which record a substantial deepening of the area over the last 400 kyr. Subsidence exceeds the average rate of sediment supply, and explains the aggradational stacking pattern of the last four 100 kyr depositional sequences and the overall backstepping of their landward pinch-out [*Trincardi and Correggiari*, 2000; *Ridente and Trincardi*, 2002].

[33] While subsidence rates appear quite constant during the interval encompassed by PRAD1.2 borehole, sediment supply changed between 0.2 and 0.8 mm/yr (Figure 6). In particular, two main peaks in sediment flux are recorded during the lowstands of MIS 10 and MIS 2. These significantly increased sediment accumulation rates have two different origins: during MIS 10 the high sediment flux reflects a proximal sediment entry point (delta or prograding shoreline) which is consistent with the very shallow paleowater depth at that time; during MIS 2, instead, the site is already in 65 m of water depth even during a sea level lowstand (Table 5). The increase of the accumulation rate during MIS 2.2 reflects the influence of the rapidly advancing Po River lowstand delta toward the southern flank of the MAD, resulting in about 10 m of sediment accumulation at the site where PRAD1.2 borehole was retrieved (see Figure 11) and greater than 200 m in the northern side of the MAD (see Figure 2). Figure 11 shows a simplified scheme of the late Quaternary central Adriatic stratigraphy, related to sediment supply fluctuations and sea level oscillations. It is important to underline the relations between the unconformities and the onlapping units, in particular those deposited during MIS 2 and MIS 10 lowstands. The MIS 2

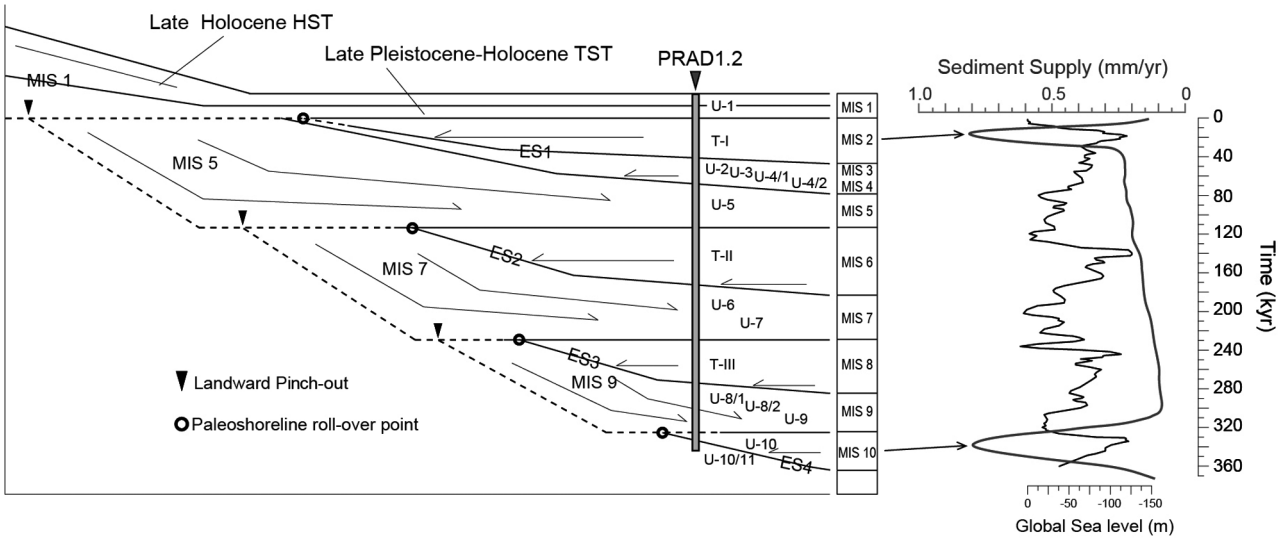

Figure 11. (left) Schematic representation of the stratigraphic relationship between progradational units on the shelf and onlapping units on the upper slope (modified from *Ridente et al.* [2008]). Dashed lines are the major unconformities (sequence boundaries). (right) Sediment supply fluctuations obtained from borehole PRAD1.2 (gray line) and global sea level oscillations (black line, modified from *Lea et al.* [2002]). The two peaks in sediment supply corresponding to sea level falls during MIS 2 and MIS 10 are correlated to the most important progradations of the late Quaternary units.

onlapping unit rests on the conformable correlative of the erosional surface, whereas during MIS 10 the erosional unconformity reached a more seaward position and affected the lowstand deposits, as highlighted by the borehole stratigraphy (see Figures 2 and 3).

[34] Previous estimates of the subsidence in the central Adriatic Sea should also be considered with caution. As an example, *Colantoni et al.* [1989] provided a subsidence rate of 3.5 mm/yr based on a single ^{14}C date of an organic-rich layer found in 200 m of water depth and interpreted as a peat layer deposited during the last glacial lowstand. However, this organic-rich layer, containing benthic foraminifera assemblage indicating riverine runoff [*Colantoni et al.*, 1989] is encased in marine sediment and most likely represents a level enriched in organic matter during MIS 2 (~LGM) on the floor of a semi-isolated basin because of the lowstand sea level and probably strongly influenced by riverine input, as also supported by similar inferences from nearby sediment cores [*Asioli*, 1996]. Moreover, the seismic stratigraphy of the area is characterized by plain-parallel reflectors that are not expected in a coastal-lagoon environment where a peat layer may form.

[35] The subsidence rates in the central Adriatic are also likely to vary laterally in response to changing tectonic/sediment load forcing. The maps of the lowstand shorelines of the four regressive sequences show that their positions along the central Adriatic margin and landward of PRAD1.2 borehole, become closer to each other proceeding to the NW suggesting that subsidence rates likely increase in this direction (Table 4 and Figure 9).

5.2. Regional Subsidence Patterns in the Adriatic Basin

[36] The area where PRAD1.2 was retrieved is considered a subsiding foredeep basin in contrast with the Apulia swell, located further south, that has been uplifted over the last 800 kyr, probably as a consequence of the lower penetration of the subducted slab, which is due to a thicker continental lithosphere [*Royden et al.*, 1987; *Doglioni et al.*, 1994]. Overall, the northern Adriatic Sea shows strong subsidence, greater in the area of Venice and Ravenna, which reflects geodynamic forcing, and is probably due to the eastward rollback of the subduction hinge [*Doglioni et al.*, 1994]. In addition to the geodynamic driving forces, it is important to consider the subsidence due to the load of the late Pleistocene to Holocene sediments, and, especially in the northern sector of the Adriatic margin, the glacio-isostatic rebound [*Antonioli et al.*, 2009].

[37] The north Adriatic has been investigated in order to quantify the rate of subsidence over long intervals (middle and late Pleistocene), and for the last century, to assess the impact of the anthropogenic subsidence, in particular in the subsiding areas of Venice and Ravenna [*Carminati et al.*, 2003; *Tosi et al.*, 2007] (Figure 1). The Venice area shows a subsidence rate between 0.18 and 0.36 mm/yr, averaged over the last million year, reaching a maximum value of 1.3 mm/yr for the late Pleistocene to Holocene, that most likely reflects sediment compaction taking place over few millennia after deposition [*Kent et al.*, 2002]. For the last 125 kyr, a complementary subsidence rate can be quantified on the basis of the work of *Massari et al.* [2004], who described the stratigraphy of two complementary boreholes (VE1 and VE1-bis) following the results of *Kent et al.* [2002]. The stratigraphy of the borehole is characterized, at 77.8 m below the ground level (which is 2 m above sea level) by shallow marine environments, ascribed to the last sea level highstand (Eemian), which gives a subsidence rate of 0.6 mm/yr for the last 125 kyr.

[38] In the Po River coastal plain north of Ravenna (Figure 1), the 173 m long continuous borehole S17

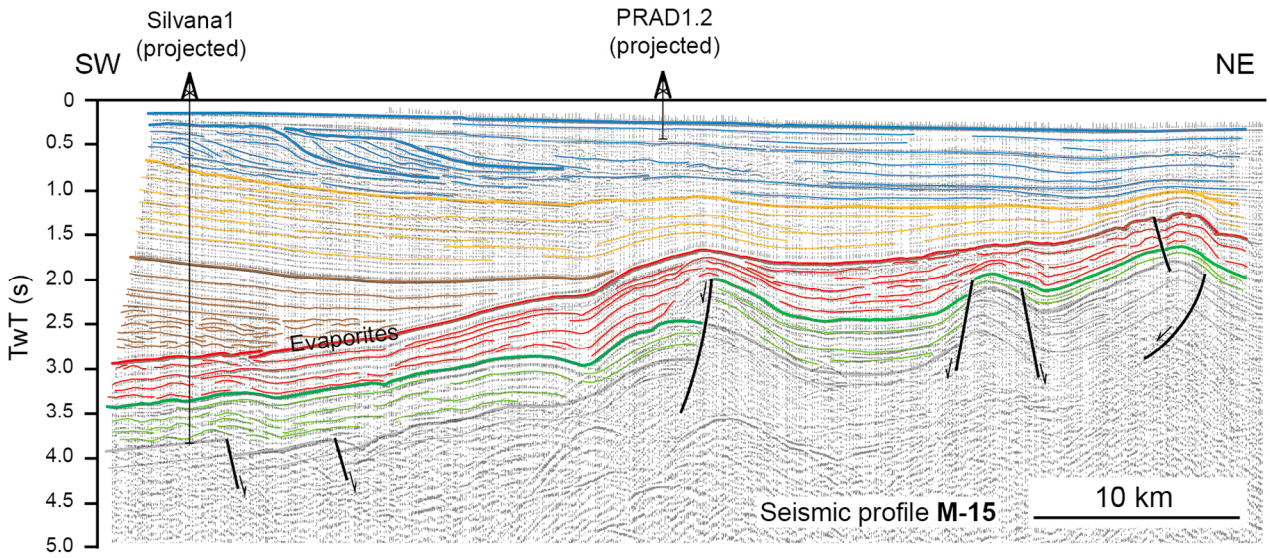

Figure 12. Interpretation of the multichannel seismic line CROP M-15 (modified from *Scrocca* [2006]) showing the stratigraphy and the main tectonic structures of the central Adriatic foredeep. Note the landward (SW) flexure of the deepest deposits, depending on the subduction of the Adria plate under the African plate, in the classical scheme of an active margin. This scheme is opposed to the youngest deposit (upper Quaternary) showing a basinward tilt typical of a passive margin. Blue unit is outer shelf to basin plain deposits (late Pleistocene to late Pliocene); yellow unit is hemipelagites and turbidites (late to middle Pliocene); brown unit is hemipelagites and turbidites (middle Pliocene to late Miocene); top red unit is evaporites (Messinian); red unit is marls and pelagic limestone (late Miocene to Early Cretaceous, Albian); green unit is cherty limestones and marls (Early Cretaceous to Early Jurassic, Lias); and grey unit is shallow water carbonates (Early Jurassic to Late Triassic, Norian). TwT, two-way travel time.

encompasses continental and marine deposits from MIS 7 to the Holocene [*Amorosi et al.*, 1999, 2004]. Facies assemblages, faunal and pollen associations allow the identification of shallow marine deposits originated during the Eemian sea level highstand 120 m below the ground. The extrapolated subsidence rate is therefore on the order of 1 mm/yr.

[39] *Ferranti et al.* [2006], on the basis of the identification of past highstand deposits, reconstructed the differentiated tectonic trends of the Italian coasts for the last 125 kyr. More detailed information, but only for the Holocene, is given by *Lambeck et al.* [2004], who tried to extract the eustatic curve. The results obtained by these authors show that the Italian coasts are characterized by variable tectonic styles; in particular referring to the Adriatic sector, the northern part is characterized by maximum subsidence rates on the order of 1.2 mm/yr, while the southern part, the Apulia swell, is characterized by uplift rate on the order of 0.2–0.3 mm/yr. The only data gap is represented by about 300 km along the central Adriatic margin, investigated in this work. The central Adriatic shelf, dominated by a subsidence rate of 0.3 mm/yr, seems to be a zone of transition between the highly subsiding northern area and the uplifting southern area.

5.3. Subsidence Rates on Foreland Versus Passive Margins

[40] Distinctive patterns of deposition in active versus passive margins, discussed by several authors [*Jordan and Flemings*, 1991; *Posamentier and Allen*, 1993], reflect the evidence that in foreland basins the subsidence-deposition ratio increases landward, while on passive margins the trend is opposite. *Rabineau et al.* [2006] used the depths of past lowstand shorelines to investigate the subsidence of the passive margin of the Gulf of Lion. The results show that the margin is characterized by a seaward progradation of the last five depositional sequences, since the glacial lowstand of MIS 12, indicating that the sediment delivered is greater than the accommodation space created (Figure 8). This observation can be explained considering that the Gulf of Lion is a passive margin, thermally cold and seismically inactive, showing a low subsidence rate principally caused by sediment load itself [*Tesson et al.*, 2005].

[41] The Adriatic margin behaves as an active margin, with subsidence-deposition ratio increasing landward, but only referring to a long time interval (millions of years). This fact is clear when observing the CROP seismic profile M-15 showing a landward tilt of the Messinian unconformity, and underlying strata, toward the Apennine chain (Figure 12; modified from *Scrocca* [2006]). On a shorter timescale, like the 300–400 kyr encompassed by borehole PRAD1.2, the Adriatic foreland shows a behavior similar to that of a passive margin that is tilting seaward. Since the sediment supply is not sufficient to exploit all the accommodation space induced by subsidence, the shoreline break of each lowstand interval moves progressively landward (Figures 8 and 9). This subsidence-driven pattern of deposition mirrors the typical pattern of a young passive margin under a significant seaward tilt.

[42] The substantial difference between the Gulf of Lion and the Adriatic margin, even if the overall geodynamic

contexts are different (passive versus active margins), is the subsidence/sedimentation ratio, which is greater in the Adriatic Sea and explains the larger landward shift of the landward pinch-outs and the backstepping of the last four depositional sequences.

5.4. Methodological Considerations

[43] To achieve accurate reconstructions of the tectonic history of a subsiding continental margin on short timescale and with high-resolution data sets, it is important to integrate different approaches, from purely analytical methods to geophysical reconstructions and paleontological/stratigraphic evidences. A particularly interesting result is that the proposed reconstructions document, for the first time, that subtle but significant changes in subsidence rate over small spatial and timescales can be resolved by high-resolution stratigraphic data in shallow slope environments (Tables 4 and 5).

[44] The backstripping procedure was introduced to investigate the evolution of a margin over intervals of tens to hundreds of millions of years and on kilometric stratigraphic sections [e.g., *Van Hinte*, 1978], in order to separate within the total subsidence the tectonic contribution and the sediment load. In the case of PRAD1.2 borehole, the backstripping procedure is still applicable and the results obtained are consistent with the results obtained with an independent method, even if significant error bars should accompany the paleowater depth reconstructions. The geohistory analysis and the application of backstripping procedure poses many problems if applied to the study of short boreholes, in particular in a time interval dominated by high-amplitude sea level fluctuations. Even if errors introduced in the decompaction calculations can be omitted, especially when porosity logs are available, the main source of error can be ascribed to the uncertainties in the reconstruction of paleowater depth and to the lithospheric response to rapid load changes driven by sea level fluctuations. Errors in paleowater depth reconstructions can be reduced by referring to long boreholes, encompassing shallow water deposits from shoreface-lagoon to midshelf environments, better defined by the benthonic communities compared to deeper water environments.

6. Conclusions

[45] By integrating two complementary geophysical and seismic-stratigraphic approaches, this paper attempts to a reconstruction of the geological history of the central Adriatic margin disentangling subsidence, eustacy and sediment-flux variations over the last 400 kyr. The results are based on the PRAD1.2 borehole, a 71.2 m continuous core, encompassing a continuous record through the last four Quaternary glacial-interglacial cycles.

[46] The geohistory analysis is first adopted to estimate the contribution of tectonic subsidence rates (0.27 mm/yr) in the total subsidence of the central Adriatic margin (0.3 mm/yr), and then compared with the subsidence rates obtained with an independent method based on the identification of dated lowstand shorelines, also resulting in a total subsidence rate of 0.3 ± 0.08 mm/yr, averaged over the last ~340 kyr. The use of lowstand shorelines made it possible to better constrain the subsidence rates and error bars associated, giving also a detailed spatial resolution on different timescales.

[47] Using the calculated subsidence rate and taking into account sediment supply fluctuations and sea level, it was possible to estimate the paleowater depths in PRAD1.2 during the last four glacial intervals, since the glacial lowstand of MIS 10. The results obtained document a progressive deepening of the central Adriatic margin at the site of the borehole at each successive lowstand. This trend is confirmed by foraminifera assemblages showing an evolution of the depositional environment from inner shelf to mid-outer shelf conditions, followed by a progressive shoaling, during MIS 2, caused by the increased sediment flux from the Po River lowstand drainage system.

[48] The Adriatic margin shows differentiated tectonic styles from north to south, depending on the different thicknesses of the subducting lithosphere. A high subsidence rate, on the order of 1 mm/yr, characterizes the northernmost part of the basin, in marked contrast with the uplift (~0.4 mm/yr) of the Apulian region in the south. The central Adriatic basin, where the borehole PRAD1.2 is located, appears to subside at 0.3 mm/yr and can be considered as a transition area between the high subsidence values of the northern Adriatic and the uplift of the south. This rate is only partially compensated by the sediment flux from the catchment and explains the overall backstepping of the Pleistocene regressive sequences along the western margin of the central Adriatic, mimicking the stratigraphic pattern typical of a young passive continental margin.

Appendix A

A1. Decompaction

[49] Following *Athy* [1930] and *Sclater and Christie* [1980], the porosity-depth relation for normally pressured sediments follows an exponential law (Figure A1):

$$\Phi = \Phi_0 \cdot e^{-cz}, \tag{A1}$$

with the following decompaction parameters: Φ_0 is initial porosity, c is porosity coefficient ($[c] = m^{-1}$), and z is depth of interest ($[z] = m$).

[50] The c coefficient is calculated by fitting the porosity value obtained by the sonic log performed parallel to the drilling of the borehole PRAD1.2. In order to minimize the error, two values of c are taken into account by using two different exponential fitting of the porosity values: one from 0 to 25 m and one from 25 to 71.2 m (Figure A1). This simplification is commonly adopted even where discrete intervals show inversions in their porosity with depth.

[51] The *second step* is to calculate the decompacted thickness of each unit. A unit of thickness T_N is buried at a depth d_N. We want to know the thickness of the unit (T_0) at some earlier time, when the unit was buried only to a depth of d_0 (Figure A2). The basic assumptions are that the porosity decreases exponentially with depth and the volume of rock grains within the unit does not change:

$$\int_{d_0}^{d_0+T_0} (1-\Phi)dz = \int_{d_N}^{d_N+T_N} (1-\Phi)dz. \tag{A2}$$

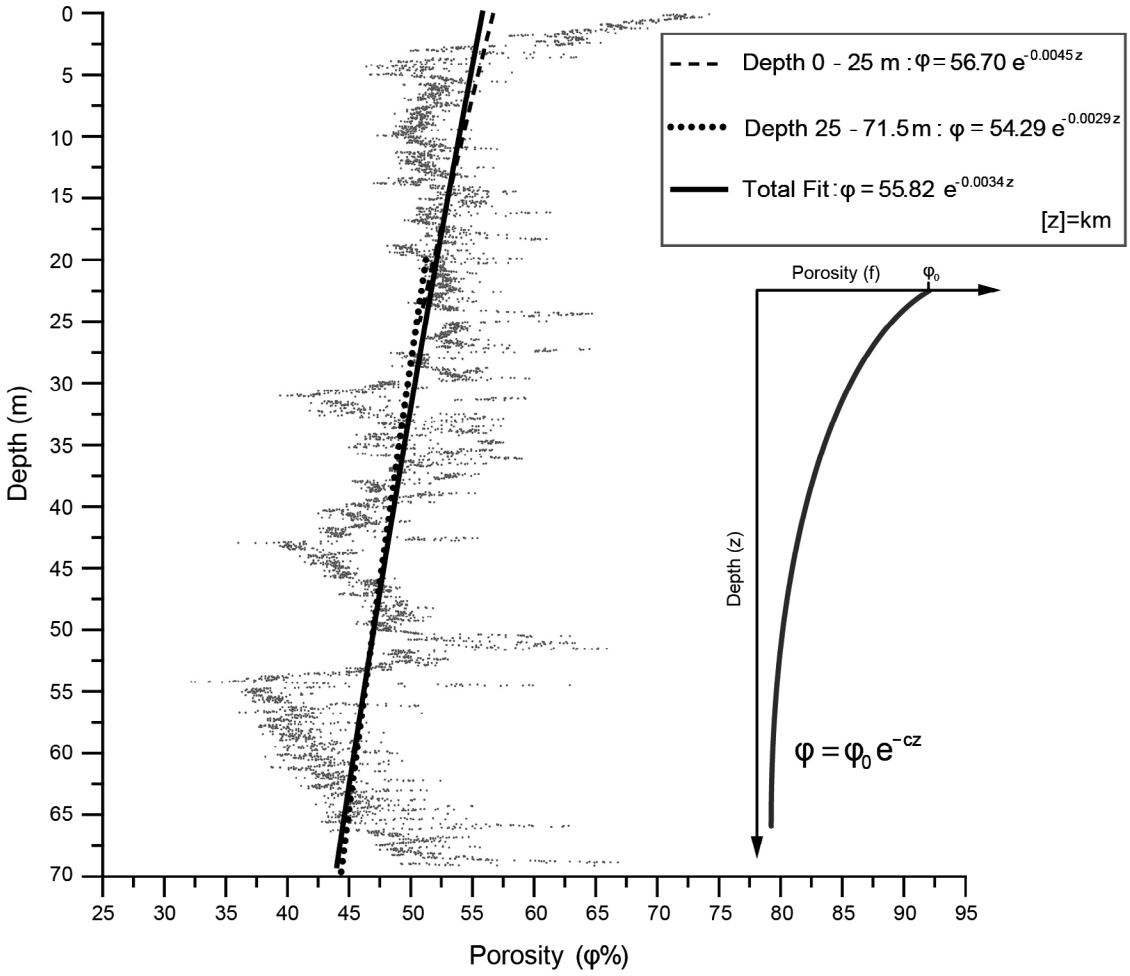

Figure A1. PRAD1.2 porosity-depth values obtained indirectly from gamma-density log calculated using a multisensor core logger (Geotek). The legend shows three compaction curves used to extrapolate the decompacted porosity and the bulk density. The solid line fits the entire borehole data. In order to minimize the error, two different compaction curves (dashed and dotted lines) are used for two intervals: 0–25 m depth and 25 m to the bottom of the borehole. The compaction coefficient (c) reflects the compaction behavior: the higher the c value, the faster the sediment is compacted. The diagram on the right shows theoretical porosity versus depth.

These two integrals can be evaluated analytically, knowing that

$$\Phi_N = \Phi_0 \exp(-cz). \tag{A3}$$

$$\begin{aligned}\int_{d_0}^{d_0+T_0}(1-\Phi)dz &= \int_{d_0}^{d_0+T_0}(1-\Phi_0\cdot e^{-cz})dz \\ &= \int_{d_0}^{d_0+T_0} dz - \Phi_0\int_{d_0}^{d_0+T_0}(e^{-cz})dz \\ &= [z]_{d_0}^{d_0+T_0} + \frac{\Phi_0}{c}[e^{-cz}]_{d_0}^{d_0+T_0} \\ &= T_0 + \frac{\Phi_0}{c}e^{-cd_0}\cdot\left(e^{-cT_0}-1\right).\end{aligned} \tag{A4}$$

By applying the same method for the right side of the equation, we obtain

$$T_0 + \frac{\Phi_0}{c}e^{-cd_0}\cdot\left(e^{-cT_0}-1\right) = T_N + \frac{\Phi_0}{c}e^{-cd_N}\cdot\left(e^{-cT_N}-1\right). \tag{A5}$$

It is impossible to solve equation (A5) directly for T_0; this is an example of transcendental equation. The best approximate solution can be obtained by isolating T_0 and assuming a value for it, and then calculating a new value for T_0. This process is repeated until T_0 stops changing from one step to the next. The resulting value is the solution.

[52] Isolating T_0 from equation (A5) gives

$$T_0 = -\frac{\Phi_0}{c}e^{-cd_0}\cdot\left(e^{-cT_0}-1\right) + T_N + \frac{\Phi_0}{c}e^{-cd_N}\cdot\left(e^{-cT_N}-1\right), \tag{A6}$$

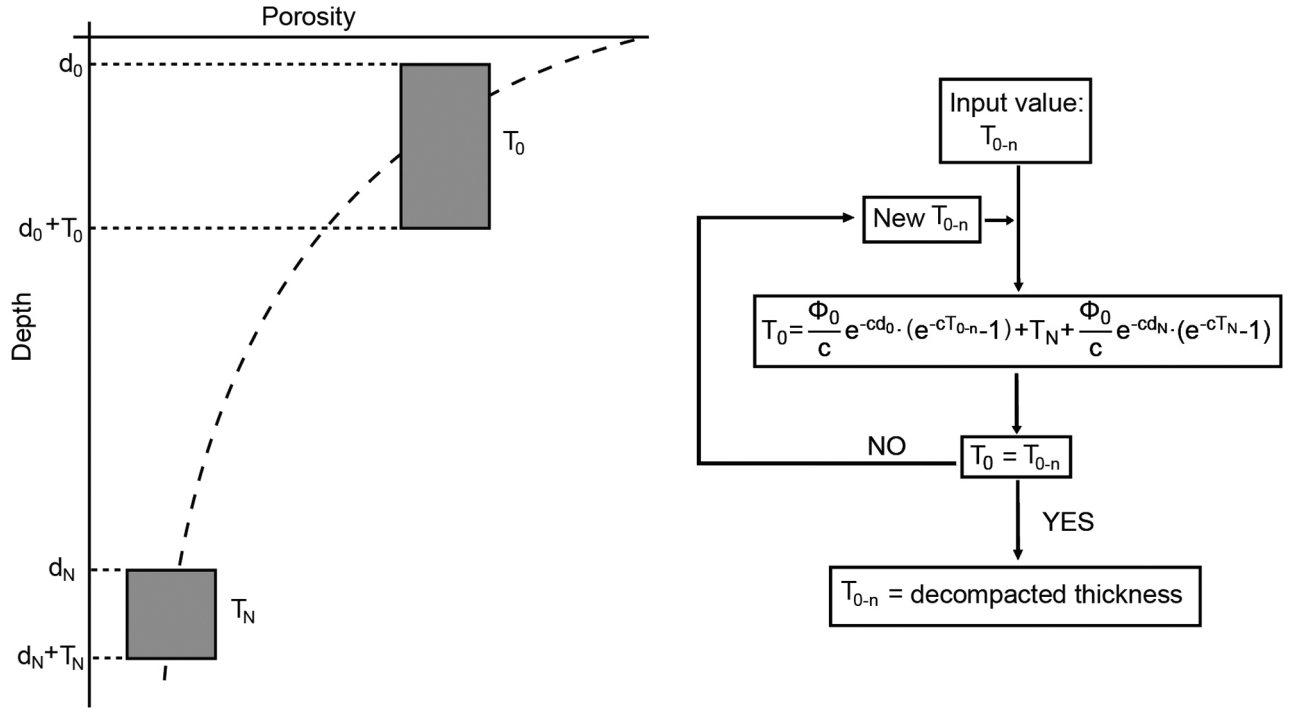

Figure A2. (left) Diagram showing the decompaction procedure. The upper and lower boundaries of each sedimentary unit (gray boxes) are introduced in the equations. (right) Algorithm to evaluate the decompacted depth; for each cycle, the algorithm tends toward the final decompacted value until the result stops changing.

where T_0 is thickness after decompaction ($[T_0]$ = m), T_N is initial thickness ($[T_N]$ = m), d_0 is new burial depth ($[d_0]$ = m), d_N is burial depth ($[d_N]$ = m), Φ_0 is initial porosity, and c is porosity constant ($[c] = m^{-1}$).

[53] A reasonable estimate for T_0 is the modern thickness, measured in the borehole. By introducing this value on the right side of equation (A6), we obtain the first value of decompacted thickness. The process has to be repeated until T_0 converges to a stable value, following the algorithm defined in Figure A2. Table A1 and Figure 5 show the decompacted depths.

A2. Isostasy

[54] In the classical scheme of Airy isostasy [*Airy*, 1855], changes in topographic relief or seafloor elevation are compensated locally by changes in crustal thickness. An Airy compensation assumes a lithosphere with zero lateral strength: if a surface load is applied, the crust behaves as a series of vertical-sided prisms, where shear stresses cannot be transmitted from one prism to the adjacent ones.

[55] The weight of a column of sediment of uniform section is directly proportional to the bulk density, that is the

Table A1. Decompaction Process[a]

Unit Name	Age (kyr)															
	340	331	315	263	248	225	184	143	125	68	61	57.5	27.3	17.5	7.2	0
U-10/11	13.368	19.81	21.783	25.043	29.716	32.521	38.195	41.94	44.173	53.709	54.899	55.445	60.461	66.162	70.415	71.2
U-10	0	6.72	8.776	12.171	17.033	19.949	25.842	29.728	32.043	41.919	43.151	43.716	48.907	54.792	59.189	60
U-9	0	0	2.101	5.57	10.536	13.513	19.525	23.487	25.846	35.905	37.159	37.734	43.019	49.002	53.476	54.2
U-8/2	0	0	0	3.492	8.491	11.487	17.537	21.523	23.888	34.006	35.267	35.845	41.16	47.174	51.672	52.5
U-8/1	0	0	0	0	5.056	8.085	14.201	18.229	20.618	30.836	32.109	32.692	38.058	44.125	48.665	49.5
T-III	0	0	0	0	0	3.079	9.294	13.385	15.811	26.18	27.471	28.062	33.505	39.652	44.254	45.1
U-7	0	0	0	0	0	0	6.277	10.407	12.856	23.32	24.623	25.219	30.71	36.907	41.458	42.4
U-6	0	0	0	0	0	0	0	4.215	6.713	17.379	18.706	19.313	24.907	31.21	35.934	36.8
T-II	0	0	0	0	0	0	0	0	2.532	13.34	14.684	15.299	20.965	27.342	32.124	33
U-5	0	0	0	0	0	0	0	0	0	10.895	12.249	12.868	18.578	25	29.818	30.7
U-4/2	0	0	0	0	0	0	0	0	0	0	1.429	2.081	8.095	14.84	19.89	20.8
U-4/1	0	0	0	0	0	0	0	0	0	0	0	0.656	6.713	13.503	18.585	19.5
U-3	0	0	0	0	0	0	0	0	0	0	0	0	6.076	12.886	17.983	18.9
U-2	0	0	0	0	0	0	0	0	0	0	0	0	0	7.015	12.258	13.2
T-I	0	0	0	0	0	0	0	0	0	0	0	0	0	0	5.427	6.4
U-1	0	0	0	0	0	0	0	0	0	0	0	0	0	0	0	1

[a]The first column from right represents the present-day configuration of the borehole: the value corresponds to the depth of the bottom of each unit. The last value of each column represents the thickness (decompacted) of each unit at the time of deposition (see Appendix A).

Table A2. Porosity Values Used in the Decompaction Process[a]

Unit Name	Age (kyr)															
	340	331	315	263	248	225	184	143	125	68	61	57.5	27.3	17.5	7.2	0
U-10/11	0.534	0.524	0.521	0.516	0.509	0.505	0.496	0.491	0.488	0.474	0.472	0.472	0.465	0.457	0.451	0.450
U-10	0	0.539	0.536	0.531	0.523	0.519	0.510	0.504	0.501	0.486	0.485	0.484	0.477	0.468	0.462	0.461
U-9	0	0	0.543	0.537	0.530	0.525	0.516	0.510	0.507	0.492	0.490	0.489	0.482	0.474	0.467	0.466
U-8/2	0	0	0	0.542	0.534	0.529	0.520	0.514	0.510	0.496	0.494	0.493	0.485	0.477	0.471	0.470
U-8/1	0	0	0	0	0.541	0.536	0.526	0.520	0.517	0.501	0.499	0.499	0.491	0.482	0.476	0.475
T-III	0	0	0	0	0	0.542	0.532	0.526	0.522	0.507	0.505	0.504	0.496	0.487	0.481	0.480
U-7	0	0	0	0	0	0	0.540	0.533	0.529	0.513	0.511	0.510	0.502	0.493	0.487	0.485
U-6	0	0	0	0	0	0	0	0.541	0.537	0.521	0.519	0.518	0.509	0.500	0.493	0.492
T-II	0	0	0	0	0	0	0	0	0.543	0.526	0.524	0.523	0.514	0.505	0.498	0.496
U-5	0	0	0	0	0	0	0	0	0	0.536	0.534	0.533	0.524	0.514	0.507	0.505
U-4/2	0	0	0	0	0	0	0	0	0	0	0.565	0.563	0.548	0.532	0.521	0.518
U-4/1	0	0	0	0	0	0	0	0	0	0	0	0.566	0.551	0.535	0.523	0.521
U-3	0	0	0	0	0	0	0	0	0	0	0	0	0.559	0.542	0.530	0.528
U-2	0	0	0	0	0	0	0	0	0	0	0	0	0	0.558	0.545	0.543
T-I	0	0	0	0	0	0	0	0	0	0	0	0	0	0	0.560	0.56
U-1	0	0	0	0	0	0	0	0	0	0	0	0	0	0	0	0.57

[a]The last values of each column represent the porosity of the sedimentary unit at the time of deposition. The reconstructed porosity is then used to obtain the bulk density (see Table A3 and Appendix A).

density of a volume of material calculated taking into account the relationship between the volume of pores, saturated with salt water, and the volume occupied by sediment. The value of bulk density must be calculated each time the most recent unit is removed from the sediment column in the process of decompaction, taking into account changes in porosity occurring at each step. To know how the average bulk porosity of each sediment layer varies in time [*Angevine et al.*, 1990] and, consequently, to calculate the porosity of each sediment unit at its new depth, we need to solve the following, where y_1 and y_2 are the new burial depths:

$$\Phi = \frac{\Phi_0}{c}\frac{\exp(-cy_1) - \exp(-cy_2)}{y_2 - y_1}. \tag{A7}$$

Table A2 shows the results.

[56] The bulk density (ρ_b) depends on the porosity and the density of sediment grains (ρ_s). The density of the sediment grains of each unit of the modern sediment section is obtained by taking the mean value from the PRAD1.2 sonic log (Table 1). The bulk density (Table A3) can be evaluated using

$$\rho_b = \Phi\rho_w + (1 - \Phi)\rho_s, \tag{A8}$$

and the bulk density of the entire sedimentary column ($\overline{\rho}_b$) made of n units is

$$\overline{\rho}_b = \sum_i \left\{ \frac{\Phi_i\rho_w + (1 - \Phi_i)\rho_{s(i)}}{S^*} \right\} \cdot T_i^*, \tag{A9}$$

where Φ_i is the porosity of the ith Unit at the time t, $\rho_{s(i)}$ is the grain density of the same Unit ($[\rho_{s(i)}]$ = kg/m^3), T_i* is the thickness of the ith Unit ($[T_i^*]$ = m), and S* is the total thickness of the decompacted sedimentary column at the time t ($[S^*]$ = m).

[57] Once we obtain the bulk density of the sediment column in each of the stages of deposition, we can apply the Airy correction for surface loads:

$$Z = S \cdot \left(\frac{\rho_a - \overline{\rho}_b}{\rho_a - \rho_w} \right), \tag{A10}$$

where Z is depth of the basin after Airy compensation ([Z] = m), S is thickness of the removed sediment section ([S] = m), ρ_a is density of the underlying material, under the sediment section ($[\rho_a]$ = 3330 kg/m^3), $\overline{\rho}_b$ is bulk density of the sedimentary column ($[\overline{\rho}_b]$ = kg/m^3), and ρ_w is density of salt water ($[\rho_w]$ = 1030 kg/m^3).

Appendix B

[58] Foraminifera distribution has been and still is one of the most used proxy to evaluate variations in paleodepth of past depositional environment. Nevertheless, advantages

Table A3. Bulk Density of Each Unit Obtained From Decompacted Porosity Values[a]

Unit Name	Decompacted Total Thickness (m)	Bulk Density (kg/m^3)
U-1	71.2	1444.7
T-I	70.415	1446.3
U-2	66.162	1448
U-3	60.461	1447.7
U-4/1	55.445	1448.5
U-4/2	54.899	1448.7
U-5	53.709	1449
T-II	44.173	1449.6
U-6	41.94	1449.3
U-7	38.195	1446
T-III	32.521	1441.5
U-8/1	29.716	1439.5
U-8/2	25.043	1435.3
U-9	21.783	1428.4
U-10	19.81	1423.5
U-10/11	13.368	1411.6

[a]See Appendix A.

and disadvantages of this method have been highlighted by recent studies of the ecological requirements of foraminifera. Water depth cannot be per se the only limiting factor for the life of benthic foraminifera [*Van der Zwaan et al.*, 1999]; food availability (flux) and oxygen content are considered among the factors more limiting benthic foraminifera distribution (see *Jorissen* [1999] for a review). Individual species are never good paleodepth markers, even if it is possible to distinguish species typical of deep waters and others of shelf environment.

[59] In this study, the paleobathymetry estimate has been obtained evaluating the composition of the benthic foraminifera assemblage (see Tables 3 and 5; from *Piva* [2007] and *Piva et al.* [2008b]), and ascribing to each assemblage the geomorphologic context (i.e., shelf, slope) along with the bathymetric range occupied by the assemblages and based on (local) models of distribution of the modern benthic foraminifera in the Adriatic Sea [*Jorissen*, 1988, 1987; *Van der Zwaan and Jorissen*, 1991; *Barmawidjaja et al.*, 1992; *De Stigter et al.*, 1998; *Morigi et al.*, 2005] and Mediterranean [*De Rijk et al.*, 1999]. However, the application of local bathymetric zonations has some limitations, as the absolute numerical estimates of depth are dependent on local flux variation [*Van der Zwaan et al.*, 1999]. In Tables 3 and 5 the benthic foraminifera assemblages are expressed by three ranks of abundance from which the bathymetric range has been obtained following the subsequent classification: in bold italics are reported the most abundant taxa (>20%), in underlined italics the common taxa (5–10%) and in italics the taxa with abundances between 1 and 5%. Moreover, it is necessary to consider that PRAD1–2 spans approximately the last 400 kyr and in many intervals the assemblages, present during glacials and interglacials, are dominated by taxa presently living neither in the Adriatic nor in the Mediterranean (for instance *Sigmoilina sellii* in MIS 2, *Islandiella islandica* and *Elphidium excavatum* forma *clavata* in MIS 6, 8 and 10). The bathymetric range for these species had therefore to be obtained from the extra-Mediterranean literature [*Miller et al.*, 1982; *Linke and Lutze*, 1993; *Jennings et al.*, 2004; *Murray*, 2006].

[60] To get a relatively more quantitative paleowater depth estimate, we also applied the formula developed by *Van der Zwaan et al.* [1990]. This method relies on the idea that planktonic and benthic foraminifera are both dependent on flux and that this dependency will be eliminated using the ratio between the two. The proposed formula is D = ln (a + b %P), with D = depth, a = 3.58718, b = 0.03534; %P = P/P + (B-infaunal), where P = number of planktic foraminifera specimens and B = number of benthic foraminifera specimens. The "a" and "b" values implies that if P = 100 the estimated paleobathymetry is 1250 m, while if P = 0 D is 36 m. Moreover, this method assumes negligible the dissolution of the tests and reworked specimens should not be counted and used for this purpose. As shown in the formula, the benthic term must be corrected for the presence of genera with infaunal habitat, such as *Bulimina*, *Globobulimina*, *Bolivina*, *Uvigerina* and *Fursenkoina*.

[61] In the first method described, the reconstructed bathymetric range does not depend on planktic foraminifera abundance; the method was applied to double-check the values obtained following *Van der Zwaan et al.* [1990], and, at places, to estimate paleodepth in intervals where *Van der Zwaan et al.*'s [1990] formula proved not applicable (for instance in environments shallower than 40 m and during sapropel events.).

[62] **Acknowledgments.** This study was supported by the EU project PROMESS1 (EVR1-2001-41), funded within the 5th Framework Programme. Antonio Cattaneo thanks ISMAR-CNR for financial support during a 6-month sabbatical leave in Bologna. We are grateful to Alessandro Amorosi and an anonymous reviewer for reviewing the manuscript and providing useful comments and suggestions. We also thank Eugenio Carminati for his help and interesting discussions on this subject and Marco Ligi, Valentina Ferrante, Marzia Rovere, and Elisabetta Campiani for their support on seismic processing and mapping. This is CNR- ISMAR Bologna contribution 1649.

References

Airy, G. B. (1855), On the computation of the effect of the attraction of mountain masses, *Philos. Trans. R. Soc. London*, *145*, 101–104, doi:10.1098/rstl.1855.0003.

Allen, P. A., and J. R. Allen (1990), *Basin Analysis, Principles and Applications*, 451 pp., Blackwell Sci., Cambridge, U.K.

Amorosi, A., M. L. Colalongo, F. Fusco, G. Pasini, and F. Fiorini (1999), Glacio-eustatic control of continental–shallow marine cyclicity from Late Quaternary deposits of the southeastern Po Plain, northern Italy, *Quat. Res.*, *52*, 1–13, doi:10.1006/qres.1999.2049.

Amorosi, A., M. L. Colalongo, F. Fiorini, F. Fusco, G. Pasini, S. C. Vaiani, and G. Sarti (2004), Palaeogeographic and palaeoclimatic evolution of the Po Plain from 150-ky core records, *Global Planet. Change*, *40*, 55–78, doi:10.1016/S0921-8181(03)00098-5.

Angevine, C. L., P. L. Heller, and C. Paola (1990), *Quantitative Sedimentary Basin Modeling*, *Educ. Course Notes*, vol. 32, 247 pp., Am. Assoc. of Pet. Geol., Tulsa, Okla.

Antonioli, F., et al. (2009), Holocene relative sea-level changes and vertical movements along the Italian and Istrian coastlines, *Quat. Int.*, *206*, 102–133, doi:10.1016/j.quaint.2008.11.008.

Asioli, A. (1996), High resolution foraminifera biostratigraphy in the Central Adriatic basin during the last deglaciation: A contribution to the PALICLAS Project, in *Palaeoenvironmental Analysis of Italian Crater Lake and Adriatic Sediments*, edited by F. Oldfield and P. Guilizzoni, *Mem. Ist. Ital. Idrobiol.*, *55*, 197–218.

Asioli, A., F. Trincardi, J. J. Lowe, D. Ariztegui, L. Langone, and F. Oldfield (2001), Sub-millennial scale climatic oscillations in the central Adriatic during the Lateglacial: Palaeoceanographic implications, *Quat. Sci. Rev.*, *20*, 1201–1221, doi:10.1016/S0277-3791(00)00147-5.

Athy, L. F. (1930), Density, porosity, and compaction of sedimentary rocks, *Am. Assoc. Pet. Geol. Bull.*, *14*, 1–24.

Bard, E., B. Hamelin, and R. G. Fairbanks (1990), U-Th ages obtained by mass spectrometry in corals from Barbados: Sea level during the past 130,000 years, *Nature*, *346*, 456–458, doi:10.1038/346456a0.

Barmawidjaja, D. M., F. J. Jorissen, S. Puskaric, and G. J. Van der Zwaan (1992), Microhabitats selection by benthic foraminifera in the northern Adriatic Sea, *J. Foraminiferal Res.*, *22*(4), 297–317, doi:10.2113/gsjfr.22.4.297.

Bassinot, F. C., L. D. Labeyrie, E. Vincent, X. Quidelleur, N. J. Shackleton, and Y. Lancelot (1994), The astronomical theory of climate and the age of the Brunhes Matuyama magnetic reversal, *Earth Planet. Sci. Lett.*, *126*, 91–108, doi:10.1016/0012-821X(94)90244-5.

Berger, A., and M. F. Loutre (1991), Insolation values for the climate of the last 10 million years, *Quat. Sci. Rev.*, *10*, 297–317, doi:10.1016/0277-3791(91)90033-Q.

Carminati, E., C. Doglioni, and D. Scrocca (2003), Apennines subduction-related subsidence of Venice (Italy), *Geophys. Res. Lett.*, *30*(13), 1717, doi:10.1029/2003GL017001.

Carminati, E., L. Corda, G. Mariotti, and M. Brandano (2007), Tectonic control on the architecture of a Miocene carbonate ramp in the central Apennines (Italy): Insights from facies and backstripping analyses, *Sediment. Geol.*, *198*, 233–253, doi:10.1016/j.sedgeo.2006.12.005.

Cattaneo, A., and F. Trincardi (1999), The late-Quaternary transgressive record in the Adriatic epicontinental sea: Basin widening and facies partitioning, in *Isolated Shallow Marine Sand Bodies: Sequence Stratigraphic Analysis and Sedimentologic Interpretation*, edited by K. Bergman and J. Snedden, *Spec. Publ. SEPM Soc. Sediment. Geol.*, *64*, 127–146.

Cattaneo, A., A. Correggiari, L. Langone, and F. Trincardi (2003), The late-Holocene Gargano subaqueous delta, Adriatic shelf: Sediment pathways and supply fluctuations, *Mar. Geol.*, *193*, 61–91, doi:10.1016/S0025-3227(02)00614-X.

Cattaneo, A., F. Trincardi, A. Asioli, and A. Correggiari (2007), The western Adriatic Shelf Clinoform: Energy-limited bottomset, *Cont. Shelf Res.*, *27*, 506–525, doi:10.1016/j.csr.2006.11.013.

Chappell, J., and N. J. Shackleton (1986), Oxygen isotopes and sea level, *Nature*, *324*, 137–140, doi:10.1038/324137a0.

Colantoni, P., A. Asioli, A. M. Borsetti, L. Capotondi, and C. Vergnaud-Grazzini (1989), Subsidenza tardo-pleistocenica ed olocenica nel medio Adriatico evidenziata dalla geofisica e da ricostruzioni paleoambientali, *Mem. Soc. Geol. Ital.*, *42*, 209–220.

De Rijk, S., S. R. Troelstra, and E. J. Rohling (1999), Benthic foraminiferal distribution in the Mediterranean Sea, *J. Foraminiferal Res.*, *29*, 93–103.

De Stigter, H. C., F. J. Jorissen, and G. J. Van der Zwaan (1998), Bathymetric distribution and microhabitat partitioning of live (Rose Bengal stained) benthic foraminifera along a shelf to deep sea transect in the southern Adriatic Sea, *J. Foraminiferal Res.*, *28*, 40–65.

Doglioni, C., F. Mongelli, and P. Pieri (1994), The Puglia uplift (SE Italy): An anomaly in the foreland of the Apenninic subduction due to buckling of a thick continental lithosphere, *Tectonics*, *13*, 1309–1321, doi:10.1029/94TC01501.

Ferranti, L., et al. (2006), Markers of the last interglacial sea-level high stand along the coast of Italy: Tectonic implications, *Quat. Int.*, *145–146*, 30–54, doi:10.1016/j.quaint.2005.07.009.

Jennings, A. E., N. J. Weiner, G. Helgadottir, and J. T. Andrews (2004), Modern foraminiferal faunas of the Southwestern to Northern Iceland shelf: Oceanographic and environmental controls, *J. Foraminiferal Res.*, *34*(3), 180–207, doi:10.2113/34.3.180.

Jordan, T. E., and P. B. Flemings (1991), Large-scale stratigraphic architecture, eustatic variation, and unsteady tectonism: A theoretical evaluation, *J. Geophys. Res.*, *96*, 6681–6699, doi:10.1029/90JB01399.

Jorissen, F. J. (1987), The distribution of benthic foraminifera in the Adriatic Sea, *Mar. Micropaleontol.*, *12*, 21–48, doi:10.1016/0377-8398(87)90012-0.

Jorissen, F. J. (1988), Benthic foraminifera from the Adriatic Sea: Principles of phenotypic variation, *Utrecht Micropaleontol. Bull. 37*, 174 pp., Utrecht, Netherlands.

Jorissen, F. J. (1999), Benthic foraminiferal microhabitats below the sediment-water interface, in *Modern Foraminifera*, edited by B. K. Sen Gupta, pp. 161–180, Kluwer Acad., Dordrecht, Netherlands.

Jouet, G., S. Berné, M. Rabineau, M. A. Bassetti, P. Bernier, B. Dennielou, F. J. Sierro, J.-A. Flores, and M. Taviani (2006), Shoreface migrations at the shelf edge and sea-level changes around the Last Glacial Maximum (Gulf of Lions, NW Mediterranean), *Mar. Geol.*, *234*, 21–42, doi:10.1016/j.margeo.2006.09.012.

Kent, D. V., D. Rio, F. Massari, G. Kukla, and L. Lanci (2002), Emergence of Venice in the Pleistocene, *Quat. Sci. Rev.*, *21*, 1719–1727, doi:10.1016/S0277-3791(01)00153-6.

Laj, C., C. Kissel, and A. P. Roberts (2006), Geomagnetic field behavior during the Iceland Basin and Laschamp geomagnetic excursions: A simple transitional field geometry?, *Geochem. Geophys. Geosyst.*, *7*, Q03004, doi:10.1029/2005GC001122.

Lambeck, K., F. Antonioli, A. Purcell, and S. Silenzi (2004), Sea-level change along the Italian coast for the past 10,000 yr, *Quat. Sci. Rev.*, *23*, 1567–1598, doi:10.1016/j.quascirev.2004.02.009.

Lea, D. W., P. A. Martin, D. K. Pak, and H. J. Spero (2002), Reconstructing a 350 kyr history of sea level using planktonic Mg/Ca and oxygen isotopic records from a Cocos Ridge core, *Quat. Sci. Rev.*, *21*, 283–293, doi:10.1016/S0277-3791(01)00081-6.

Linke, P., and G. F. Lutze (1993), Microhabitat preferences of benthic foraminifera: A static concept or a dynamic adaptation to optimize food acquisition?, *Mar. Micropaleontol.*, *20*, 215–234, doi:10.1016/0377-8398(93)90034-U.

Lisiecki, L. E., and M. E. Raymo (2005), A Pliocene-Pleistocene stack of 57 globally distributed benthic $d^{18}O$ records, *Paleoceanography*, *20*, PA1003, doi:10.1029/2004PA001071.

Lourens, L. J. (2004), Revised tuning of Ocean Drilling Program Site 964 and KC01B (Mediterranean) and implications for the $d^{18}O$, tephra, calcareous nannofossil, and geomagnetic reversal chronologies of the past 1.1 Myr, *Paleoceanography*, *19*, PA3010, doi:10.1029/2003PA000997.

Martinson, D. G., N. G. Pisias, J. D. Hays, J. Imbrie, T. C. Moore, and N. J. Shackleton (1987), Age dating and the orbital theory of the ice ages: Development of a high resolution 0 to 300,000-year chronostratigraphy, *Quat. Res.*, *27*, 1–29, doi:10.1016/0033-5894(87)90046-9.

Massari, F., D. Rio, R. Serandrei Barbero, A. Asioli, L. Capraro, E. Fornaciari, and P. P. Vergerio (2004), The environment of Venice area in the past two million years, *Palaeogeogr. Palaeoclimatol. Palaeoecol.*, *202*, 273–308, doi:10.1016/S0031-0182(03)00640-0.

Meese, D. A., A. J. Gow, R. B. Alley, G. A. Zielinsky, P. M. Grootes, M. Ram, K. C. Taylor, P. A. Mayewski, and J. F. Bolzan (1997), The Greenland Ice Sheet Project 2 depth-age scale: Methods and results, *J. Geophys. Res.*, *102*, 26,411–26,423, doi:10.1029/97JC00269.

Miller, A. L., D. B. Scott, and F. S. Medioli (1982), *Elphidium excavatum* (Terquem): Ecophenotypic versus subspecific variation, *J. Foraminiferal Res.*, *12*(2), 116–144, doi:10.2113/gsjfr.12.2.116.

Morigi, C., F. J. Jorissen, S. Fraticelli, B. J. Horton, M. Principi, A. Sabbatini, L. Capotondi, P. V. Curzi, and A. Negri (2005), Benthic foraminiferal evidence for the formation of the Holocene mud-belt and bathymetrical evolution in the central Adriatic Sea, *Mar. Micropaleontol.*, *57*, 25–49, doi:10.1016/j.marmicro.2005.06.001.

Murray, J. (2006), *Ecology and Applications of Benthic Foraminifera*, Cambridge University Press, New York.

Patacca, E., and P. Scandone (2004), The Plio-Pleistocene thrust belt: Foredeep system in the southern Apennines and Sicily, in *Geology of Italy: Special Volume of the Italian Geological Society for the IGC 32 Florence 2004*, edited by V. Crescenti et al., pp. 93–129, Società Geologica Italiana, Rome, Italy.

Pieri, M., and G. Groppi (1981), Subsurface geological structure of the Po plain, Italy, *Publ. 414*, 23 pp., P. F. Geodin., Cons. Naz. delle Ric., Rome.

Piva, A. (2007), Stratigrafia ad alta risoluzione dei depositi Quaternari in Adriatico centrale e meridionale: Impatto di cambiamenti climatici a scala sub-Milankoviana sulla circolazione in Mediterraneo, Ph.D. thesis, Univ. of Bologna, Bologna, Italy.

Piva, A., A. Asioli, R. R. Schneider, F. Trincardi, N. Andersen, E. Colmenero-Hidalgo, B. Dennielou, J.-A. Flores, and L. Vigliotti (2008a), Climatic cycles as expressed in sediments of the PROMESS1 borehole PRAD1.2, central Adriatic, for the last 370 ka: 1. Integrated stratigraphy, *Geochem. Geophys. Geosyst.*, *9*, Q01R01, doi:10.1029/2007GC001713.

Piva, A., A. Asioli, N. Andersen, J. O. Grimalt, R. R. Schneider, and F. Trincardi (2008b), Climatic cycles as expressed in sediments of the PROMESS1 borehole PRAD1.2, central Adriatic, for the last 370 ka: 2. Paleoenvironmental evolution, *Geochem. Geophys. Geosyst.*, *9*, Q03R02, doi:10.1029/2007GC001785.

Posamentier, H. W., and G. P. Allen (1993), Siliciclastic sequence stratigraphic patterns in foreland, ramp-type basins, *Geology*, *21*, 455–458, doi:10.1130/0091-7613(1993)021<0455:SSSPIF>2.3.CO;2.

Rabineau, M., S. Berné, J.-L. Olivet, D. Aslanian, F. Guillocheau, and P. Joseph (2006), Paleo sea levels reconsidered from direct observation of paleoshoreline position during Glacial Maxima (for the last 500,00 yr), *Earth Planet. Sci. Lett.*, *252*, 119–137, doi:10.1016/j.epsl.2006.09.033.

Ridente, D., and F. Trincardi (2002), Eustatic and tectonic control on deposition and lateral variability of Quaternary regressive sequences in the Adriatic basin (Italy), *Mar. Geol.*, *184*, 273–293, doi:10.1016/S0025-3227(01)00296-1.

Ridente, D., and F. Trincardi (2006), Active foreland deformation evidenced by shallow folds and faults affecting late Quaternary shelf-slope deposits (Adriatic Sea, Italy), *Basin Res.*, *18*(2), 171–188, doi:10.1111/j.1365-2117.2006.00289.x.

Ridente, D., F. Trincardi, A. Piva, A. Asioli, and A. Cattaneo (2008), Sedimentary response to climate and sea level changes during the past 400 ka from borehole PRAD1.2 (Adriatic margin), *Geochem. Geophys. Geosyst.*, *9*, Q09R04, doi:10.1029/2007GC001783.

Ridente, D., F. Trincardi, A. Piva, and A. Asioli (2009), The combined effect of sea level and supply during Milankovitch cyclicity: Evidence from shallow-marine $\delta^{18}O$ records and sequence architecture (Adriatic margin), *Geology*, *37*, 1003–1006, doi:10.1130/G25730A.1.

Rohling, E. J., M. Fenton, F. J. Jorissen, P. Bertrand, G. Ganssen, and J. P. Caulet (1998), Magnitudes of sea level lowstands of past 500,000 years, *Nature*, *394*, 162–165, doi:10.1038/28134.

Royden, L. E., E. Patacca, and P. Scandone (1987), Segmentation and configuration of subducted lithosphere in Italy: An important control on thrust-belt and foredeep-basin evolution, *Geology*, *15*, 714–717, doi:10.1130/0091-7613(1987)15<714:SACOSL>2.0.CO;2.

Sclater, J. G., and P. A. F. Christie (1980), Continental stretching: An explanation of the post-mid-Cretaceous subsidence of the central North Sea basin, *J. Geophys. Res.*, *85*, 3711–3739, doi:10.1029/JB085iB07p03711.

Scrocca, D. (2006), Thrust front segmentation induced by differential slab retreat in the Apennines (Italy), *Terra Nova*, *18*, 154–161, doi:10.1111/j.1365-3121.2006.00675.x.

Shackleton, N. J. (1987), Oxygen isotopes, ice volume and sea level, *Quat. Sci. Rev.*, *6*, 183–190, doi:10.1016/0277-3791(87)90003-5.

Skene, K. I., D. J. W. Piper, A. E. Aksu, and J. P. M. Syvitski (1998), Evaluation of the global oxygen isotope curve as a proxy for Quaternary sea level by modeling of delta progradation, *J. Sediment. Res.*, *68*, 1077–1092.

Sleep, N. H. (1971), Thermal effects of the formation of Atlantic continental margins by continental break up, *Geophys. J. R. Astron. Soc.*, *24*, 325–350.

Steckler, M. S. (1999), High resolution sequence stratigraphic modeling: 1. The interplay of sedimentation, erosion and subsidence, in *Numerical Experiments in Stratigraphy: Recent Advances in Stratigraphic and Computer Simulations*, edited by J. Harbaugh et al., *Mem. 62*, pp. 139–149, Soc. of Econ. Paleontol. and Mineral., Tulsa, Okla.

Steckler, M. S., and A. B. Watts (1978), Subsidence of the Atlantic-type continental margin off New York, *Earth Planet. Sci. Lett.*, *41*, 1–13, doi:10.1016/0012-821X(78)90036-5.

Sydow, J., and H. H. Roberts (1994), Stratigraphic framework of a late Pleistocene shelf-edge delta, Northeast Gulf of Mexico, *AAPG Bull.*, *78*, 1276–1312.

Tesson, M., C. Labaune, and B. Gensous (2005), Small rivers contribution to the Quaternary evolution of a Mediterranean littoral system: The western gulf of Lion, France, *Mar. Geol.*, *222–223*, 313–334, doi:10.1016/j.margeo.2005.06.021.

Thorne, J. A., and D. J. P. Swift (1991), Sedimentation on continental margins, VI: A regime model for depositional sequences, their component systems tracts, and bounding surfaces, in *Shelf Sand and Sandstone Bodies*, edited by D. J. P. Swift et al., *Spec. Publ. Int. Assoc. Sedimentol.*, *14*, 189–255.

Tosi, L., P. Teatini, L. Carbognin, and J. Frankenfield (2007), A new project to monitor land subsidence in the northern Venice coastland (Italy), *Environ. Geol.*, *52*, 889–898, doi:10.1007/s00254-006-0530-8.

Trincardi, F., and A. Correggiari (2000), Quaternary forced regression deposits in the Adriatic basin and the record of composite sea-level cycles, in *Depositional Response to Forced Regression*, edited by D. Hunt and R. Gawthorpe, *Geol. Soc. Spec. Publ.*, *172*, 245–269.

Vail, P. R., R. Mitchum Jr., R. Todd, J. Widmier, S. Thompson III, J. Sangree, J. Bubb, and W. Hatlelid (1977), Seismic stratigraphy and global changes of sea-level, in *Seismic Stratigraphy*, edited by C. E. Payton, pp. 49–212, Am. Assoc. Petrol. Geol., Tulsa, Okla.

Van der Zwaan, G. J., and F. J. Jorissen (1991), Biofacial patterns in river-induced anoxia, in *Modern and Ancient Continental Shelf Anoxia*, edited by R. Tyson and T. Pearson, *Geol. Soc. Spec. Publ.*, *58*, 65–82.

Van der Zwaan, G. J., F. J. Jorissen, and H. C. de Stigter (1990), The depth dependency of planktonic/benthic foraminiferal ratio: Constraints and applications, *Mar. Geol.*, *95*, 1–16, doi:10.1016/0025-3227(90)90016-D.

Van der Zwaan, G. J., I. A. P. Duijnstee, M. den Dulk, S. R. Ernst, N. T. Jannink, and T. J. Kouwenhoven (1999), Benthic foraminifers: Proxies or problems? A review of paleoecological concepts, *Earth Sci. Rev.*, *46*, 213–236, doi:10.1016/S0012-8252(99)00011-2.

Van Hinte, J. E. (1978), Geohistory analysis: Application of micropaleontology in exploration geology, *AAPG Bull.*, *62*, 201–222.

Waltham, D., C. Taberner, and C. Docherty (2000), Error estimation in decompacted subsidence curves, *AAPG Bull.*, *84*, 1087–1094.

Watts, A. B., and W. B. F. Ryan (1976), Flexure of the lithosphere and continental margin basins, *Tectonophysics*, *36*, 25–44, doi:10.1016/0040-1951(76)90004-4.

A. Asioli, IGG, CNR, Via Matteotti 30, 35137 Padova, Italy.

A. Cattaneo, GM-LES, Ifremer, 29280 Plouzané, France.

V. Maselli, Dipartimento di Scienze della Terra e Geologico-Ambientali, Univerisità di Bologna, Piazza di Porta San Donato 1, 40126 Bologna, Italy. (vittorio.maselli@bo.ismar.cnr.it)

D. Ridente, IGAG, CNR, Piazzale Moro 5, 00185 Rome, Italy.

F. Trincardi, ISMAR, Istituto di Scienze Marine (CNR), Via Gobetti 101, 40129 Bologna, Italy.